Universitetet i Stavanger

**FACULTY OF SCIENCE AND TECHNOLOGY**

# BACHELOR'S THESIS

| | |
|---|---|
| Study program/specialization:<br><br>Bachelor's degree in Mechanical Engineering | Spring semester, 2021<br><br>Open / Confidential |
| Author: Alexander Falch Voerman & Sigvart Daniel Rodriguez Høien | |
| Program coordinator: Hirpa Gelgele Lemu<br><br>Supervisor(s): Hirpa Gelgele Lemu | |
| Title of bachelor's thesis:<br><br>Performance analysis of thrusters and using the concept of Design for Assembly for construction of an ROV-frame | |
| Credits (ECTS): 2 x 20 | |
| Keywords:<br><br>UiS Subsea, Remotely Operated underwater Vehicle (ROV), Design for Assembly (DFA), Thruster analysis, MATE ROV Competition, CFD, Structural analysis | Number of pages: 61<br><br>+ supplemental material/other: 20<br><br>Stavanger, 15.05.2021<br>date/year |

# Abstract

This thesis aimed to develop an ROV-frame based on the concept of Design for Assembly, while conducting a performance analysis of the thrusters to be used for its required motion. The development of the ROV-frame and the analysis of the thrusters would assist UiS Subsea in their development of the ROV to compete in the 2021 MATE ROV competition. More specifically, the frame design incorporated an iterative process where its components were analysed by how essential they were for the operation of the ROV. The concept of Design for Assembly gave good results in design efficiency and through the assembly fitment process, but worse in terms of cost, quality of design and assembly time. This is due to the fact that only one unit was produced, of which the Design for Assembly concept calculations is more aimed at a production line.

Throughout the design, considerations have been given to the implementation of external equipment from other teams in UiS Subsea. The frame had to incorporate enough space for the number of thrusters needed, and the materials needed for the frame was evaluated based on weight, tensile strength, and density. Calculations have been performed of centre of gravity and centre of buoyancy, structural calculations and analysis of screw connections, welds, 3D-printed parts, and metals used in the construction of the frame. By doing these calculations, the components used in the frame were found to be more than strong enough with a weight distribution that provides good stability under water.

Through the performance analysis of thrusters, different angles and configurations were considered, and a setup that gave the desired manoeuvrability was found. This was proved through manual vectorial calculations, which were further used in a computational fluid dynamics analysis where the dynamic properties of the frame gave good results. Through this, the ROV's coefficient of drag was derived, and a maximum speed in ideal conditions underwater was found.

# Table of content

# Foreword

This thesis is written to cover the design, the manufacture, and the assembly process of the Remotely Operated underwater Vehicle (ROV) that is to be built by UiS Subsea at the University of Stavanger (UiS), Faculty of Science and Technology. The objective of this thesis is to develop an aesthetically pleasing design using the concept of Design for Assembly (DFA), this will limit the complexity and the cost of the components of the ROV. The thesis will also cover the performance analysis of the thrusters that are to be fitted to the ROV.

Chapter 1 and 2 covers the background of the student organization UiS Subsea, insight and mission objectives of the Marine Advanced Technology Education (MATE) ROV competition, and the history and evolution of the ROV.

Chapter 3 to 5 takes the operational functionality of the ROV into consideration. Step-by-step the design, the frame structure, the thruster performance, and any choices made during the thesis are justified through manual calculations as well as computational simulations. The simulations include graphical representations of flow values and structural loads.

Chapter 6 and 7 covers the conclusion of this thesis, and additional contributions to the UiS Subsea team. Additional contributions refer to the work performed beyond the scope set for this thesis.

This thesis builds upon several contributions made by previous UiS Subsea teams in respect to design, thruster placement, and functionality. The ROV continues to evolve with respect to the MATE competition requirements, and the design philosophy of the 2021 UiS Subsea team. The ROV design represents a robust design that differs from previous years. This allows for the ROV to have an extended operational scope, that can also be used outside of the MATE competition.

By reading this thesis, the reader will get an in-depth introduction to the thought process of designing an ROV from scratch using the concept of DFA. The reader will also get an insight into the many choices that has to be made, and that will affect the overall appearance and performance of the ROV. The thesis will serve as an example of the process of designing an ROV prototype. It will also function as a guide for coming UiS Subsea team members that need inspiration for their ROV-frame.

We would like to express our sincere gratitude to the University of Stavanger (UiS), Faculty of Science and Technology, for allowing us to take part in the UiS Subsea project. Without the free use of facilities and workshop equipment, this project would have been a lot harder to accomplish. We were given a golden opportunity to showcase the knowledge gained throughout our attendance at UiS and were allowed to let our creativity shine through in the finished product.

With the support from fellow students, professors, and staff, we were able to accomplish a project of great magnitude, with a high level of intricacy into a finished prototype. We will continue to learn as we graduate from UiS, with the knowledge obtained from all of you.

Lastly, we would like to thank our loved ones, our family and friends who have stood by our side through challenging times of little to no presence, and through the worldwide pandemic of Covid-19. Without your support and constant source of motivation, our attendance at UiS would have been much more challenging.

Stavanger, 15th May 2021

*Alexander Falch Voerman*

*Sigvart Daniel Rodriguez Høien*

UiS Subsea

# List of tables



# List of figures

# Abbreviations

| | |
|---|---|
| 3D: | 3-dimensional |
| ABS: | A composition of Acrylonitrile, butadiene, and styrene |
| AC: | Alternating current |
| Autodesk Inventor: | A Computer Aided Design (CAD) software used throughout this thesis |
| Autonomous: | Being able to self-govern certain systems |
| AUV: | Autonomous Underwater Vehicle |
| BLDC: | Brushless Direct current |
| B & D: | Boothroyd and Dewhurst, a methodology in DFA |
| CAD: | Computer Aided Design |
| CFD: | Computational Fluid Dynamics |
| CNC: | Computerized Numerical Control |
| COB: | Centre of Buoyancy |
| COG: | Centre of Gravity |
| CURV: | Cable-controlled Underwater Recovery Vehicle |
| DC: | Direct current |
| DFA: | Design for assembly |
| DFM: | Design for manufacturing |
| DFMA: | Design for manufacturing and assembly |
| DFQ: | Design for quality |
| ESC: | Electronic speed controller |
| FDM: | Fused deposition manufacture |
| GPa: | Gigapascal |
| G-Code: | Geometric code |
| HCP: | Hydraulic crush pressure |
| LCD: | Liquid crystal display |
| LED: | Light-emitting diode |
| Manipulator: | Mechanical extension fitted to the ROV enabling manipulation of objects |
| MATE: | Marine Advanced Technology Education |
| Monocoque: | A construction where its load-bearing capacity is internal to its shell/frame |

| | |
|---|---|
| MPa: | Megapascal |
| N/A: | Not applicable |
| PE: | Polyethylene |
| Photomosaic: | A large-scale detailed picture/map built up by combining photos of small areas |
| PUR: | Glass Filled Polyurethane |
| ROV: | Remotely Operated Vehicle |
| SAR: | Search and Rescue |
| SLA: | Stereolithography |
| STEM: | Science, Technology, Engineering and Mathematics |
| Thruster: | Electric motor with propeller, driven within a housing |
| TIG: | Tungsten Inert Gas, a welding type useful for welding aluminium |
| UiS: | University of Stavanger |
| UV: | Ultraviolet |

# 1 Introduction

An introduction to the thesis will be given during the following sub-chapters. There is information of who UiS Subsea are and the competition that the group will be a part of as well as the vehicle that is to be built.

## 1.1 UiS Subsea

UiS Subsea is a student organization at the university of Stavanger, founded in 2013 to compete in the international MATE ROV Competition in 2014. The organization has been competing in the MATE competition every year except 2020 since its conception and continues to engage eager students writing their theses. UiS Subsea continues to push personal growth through teamwork and the use of Science Technology Engineering and Mathematics (STEM). The driving force within UiS Subsea is to function as a start-up business and involve students from several engineering disciplines to produce a finished product. The 2021 team consists of 16 dedicated students writing 8 bachelor theses within autonomous photo recognition, micro-ROV, sensor suite, power distribution, communication, manipulator, thruster control and frame and thruster analysis. This collaboration will strengthen the student's problem-solving abilities, will test their ability to work as a team towards a common goal, and will give valuable experience useful in a job after the studies.

## 1.2 MATE ROV Competition

The MATE ROV Competition is an annual student competition held at various locations throughout the United States of America and revolves around producing an ROV to perform a certain set of tasks within a set timeframe. The tasks are different from year to year and are based on challenges encountered in oceans worldwide. The mission for 2021 revolves around *The Ubiquitous Problem of Plastic Pollution*, *The Catastrophic Impact of Climate Change on Coral Reefs* and *Maintaining Healthy Waterways Part II: Delaware River and Bay* (MATE Inspiration for Innovation, 2021).

The MATE Competition began in 2001, and currently has 41 regional events that take place in the United States of America and across the world. UiS Subsea will take part in the Explorer class which is the advanced class consisting of universities, community colleges and the like (MATE Inspiration for Innovation, 2021).

## 1.3 Mission objectives

As briefly mentioned in sub-chapter *1.2 MATE ROV Competition*, the mission objectives for 2021 revolves around:

### *1.3.1 Mission 1: The Ubiquitous Problem of Plastic Pollution.*

This issue takes plastics in the oceans and especially marinas around the world into consideration. For the competition, the goal is to remove and install a type of mesh bag to a bin to passively catch floating plastics.

There will also be a need to disconnect and connect a power connector for the bin. Lastly there will be plastic pollution floating on top of the water, mid-water and at the bottom that must be removed and collected.

The second mission objective is:

### *1.3.2 Mission 2: The Catastrophic Impact of Climate Change on Coral Reefs.*

This issue revolves around the detrimental effects on the ocean's coral reefs due to climate change. For the competition, the goal is to map points of interest on the coral reef. And by using image recognition or visually inspecting the reef, determine its health based on past data. The mission also calls for removing coral fragments from a nursery structure and planting these fragments to designated locations on the coral reef. There will also be a need to stop an outbreak of *Crown of Torn* Sea stars and collect samples of sponge species for pharmaceutical research.

The third and final mission objective is:

### *1.3.3 Mission 3: Maintaining Healthy Waterways Part II: Delaware River and Bay.*

This mission call for the team to retrieve a sediment sample from inside a drainpipe and analyse for contaminants. The sample will need to be returned to the surface, and the contents analysed to determine the types of contaminant(s). The team will also have to estimate the total number of mussels in a mussel bed based on the amount found inside a quadrant that is placed on the mussel bed by the ROV. After estimating the total amount of mussels in the mussel bed, the team will have to estimate the total amount of water filtered by the mussel bed. The ROV will also have to remove a trap full of eels from a designated area and place a new empty eel trap in another designated area. Lastly the team will have to create autonomously or manually a photomosaic of a subway car that is submerged to create an artificial reef.

These three missions together with engineering, communication and safety will yield a total of 650 points, depending on how successful the overall completion of the product and mission is. The points are divided as follows:

**Product demonstrations**

- 270 points (max), plus a time bonus
- Size and weight restrictions
  - 20 points (max)
- Product demonstration organizational effectiveness
  - 10 points (max)

**Engineering & Communication**

- Technical documentation
  - 100 points (max)
- Engineering presentations
  - 100 points (max)
- Marketing displays
  - 50 points (max)
- Company Spec Sheet
  - 20 points (max)
- Corporate Responsibility
  - 20 points (max)

**Safety**

- Initial Safety and Documentation Review
  - 20 points (max)
- Safety Inspection
  - 30 points (max)
- Job Safety Analysis (JSAs)
  - 10 points (max)

## 1.4 Rules and limitations

UiS Subsea will compete in the Explorer class during the MATE ROV Competition, this means there are specific rules and limitations that adheres to the Explorer class that needs to be followed. The Explorer class is an advanced class suitable for universities, community colleges and teams that have previously attended the MATE competition. There is a need to have a deep understanding of mechanical engineering, electronics, sensors, waterproofing containers, and other technology to be able to participate in the competition.

The specific rules for the explorer class relevant for this thesis are the ones regarding weight and size. The rules affecting the frame design are given below together with Table 1.1:

- Size measurement will be made using rings with the diameters of 64 cm, 75 cm, and 92 cm and placed over the two largest dimensions of the ROV.
- Weight measurements will be conducted using a digital scale.
- Vehicles above 92 cm in diameter, or greater than 35 kg in weight will not be allowed to compete.

*Table 2.1 – MATE ROV weight and size scoring*

| Size, diameter (cm) | Available points | Weight in air (kg) | Available points |
|---|---|---|---|
| **< 64** | +10 | < 20 | +10 |
| **64.1 to 75** | +5 | 20.0 – 28 | +5 |
| **75.1 to 92** | +0 | 28.01 – 35 | +0 |

## 1.5 ROV

The term ROV, *Remotely Operated Vehicle,* is generally used for any remotely operated vehicle. The first fully developed ROV shown in Figure 1.1, *POODLE,* was created by Dimitri Rebikoff a French engineer in 1953. It was however not until the United States Navy took an interest in ROV's that the technology really took off. The US Navy created the Cable-controlled Underwater Research Vehicle (CURV) in 1963 mainly to recover sunken torpedoes, this paved the way for a brand-new era in deep sea exploration. Advancements in ROV technology continued to grow, and from a mere 20 ROV's available in 1974, there were more than 3000 ROV's operating worldwide in 1998 (The Mariners' Museum and Park, 2021).

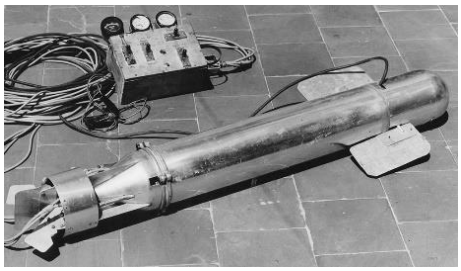

*Figure 1.1 - POODLE ROV*

Today, almost 60 years since the US Navy developed CURV, we see ROV's operating worldwide and there is heavy use of industrial ROV's in the oil and gas industry. This market is expanding into other sectors as well, including renewable energy in the form of offshore wind, wave technology as well as the private market. With the expansion in deep sea activity there is an increase in demand for innovative ROV solutions, and internationally there is a growing community of companies, student organisations and private projects that contribute to new and innovative solutions to tackle more complex tasks performed by ROV's.

*Figure 1.2 - Oceaneering' Millennium working class ROV (Oceaneering, 2021)*

UiS Subsea's ROV-frame design is based on an industrial design inspired from one of Oceaneering's ROV's (Oceaneering, 2021), shown in Figure 1.2, that is operated from a control room on a ship or an oil and gas rig. Many of the operations performed by Oceaneering' ROV's coincide very well with UiS Subsea' requirements, and so the design will be very appropriate for the tasks at hand. An ROV today is typically used for diving operations such as mapping the seabed, inspection, maintenance of seabed installations and even SAR-operations. Many of these operations would previously have been performed by deep sea divers, but as installations are placed deeper and deeper, the safety of divers can no longer be guaranteed and so there is a need for ROV's to operate and perform these tasks. The operating depth of an industrial ROV is around 3000 meters, and in some special cases down to 7000 - 8000 meters. Operating on these depths would never have been possible for deep sea divers due to the immense pressure at these depths, and so the ROV comes into its own.

The UiS Subsea team will build upon the technology developed before it, to design and build an ROV capable of reaching a depth of 100 meters. It will be able to manipulate objects, inspect subsea installations and document all of this with its onboard cameras and sensors. The reason for going beyond the 5.5-meter operating depth set by MATE is due to the challenge that arises in the development of the ROV. The team also wants a vehicle capable of extended use when not operating in the competition, this naturally increases the difficulty during the design, production and build phase.

## 1.6 Thesis contribution

Seeing there are 16 team members in the 2021 UiS Subsea team writing 8 bachelor theses, there are many depending on a ROV-frame that are both aesthetically pleasing to look at, while also being capable of carrying the needed equipment. This thesis will therefore contribute with an ROV-frame, designed with the DFA concept in mind, and a performance analysis of the thrusters that will ensure the best performance available for the ROV.

## 1.7 Scope and limitations

The thesis was limited by time, seeing that it was written during the spring semester of 2021. Due to this reason, the concepts of design, manufacturing complexity, and so on had to be limited in its scope. The product at the end was an ROV-frame prototype, designed to be capable of carrying equipment needed in the MATE competition, while adhering to the scope set by the thesis description. The ROV-frame represents a dedicated teamwork between two students, capable of delivering a finished product within all the expectations, from the scope of the thesis to the rest of the UiS Subsea team, being met.

# 2 Vehicles

## 2.1 Introduction

Choices were made early in the process of developing a design for the new ROV. These choices have valid reasons, and these reasons will be further discussed during the following chapters.

## 2.2 Former UiS Subsea ROV's

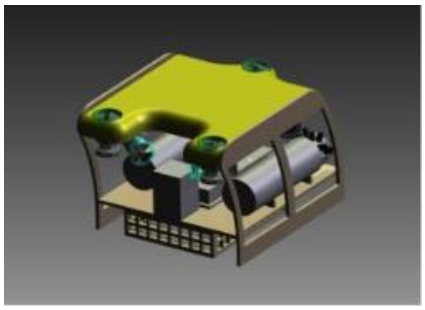

*Figure 2.1 – UiS Subsea' Njord ROV*

*Figure 2.2 – UiS Subsea' Loke ROV*

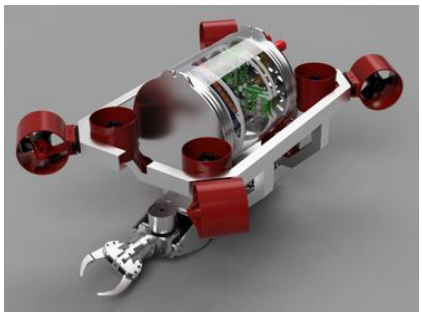

*Figure 2.3 – UiS Subsea' Ægir ROV*

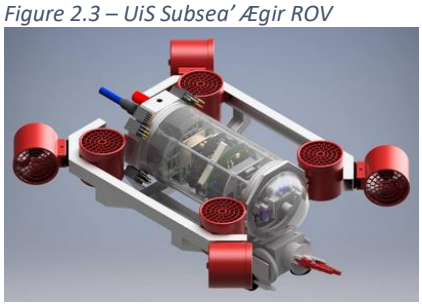

*Figure 2.4 – UiS Subsea' Vona ROV*

Looking at the design and purpose of previous ROV's, it became clear that the 2021 team wanted to do better. Previous designs, such as Njord shown in Figure 2.1 (Øydegard, 2014) incorporated a simple design, purpose built for the task at hand.

There were some variations in ROV design based on the mission, but most tasks that have been performed during the years that UiS Subsea have attended the MATE competition, required some form of motion, visual and manipulating ability. This has resulted in a design varying only slightly from year to year, starting with the 2015 Loke ROV shown in Figure 2.2, which focused on the autonomous aspect of the MATE competition. Continuing with the 2016/2017 Ægir, shown in Figure 2.3, which were a simplified and lightweight ROV. Vona, shown in Figure 2.4, was the ROV that competed in the 2018 MATE competition, and is clearly a lightweight and agile ROV (UiS Subsea, 2021).

The 2021 team wanted to change the visual and functional design, and so the 2021 ROV was radically altered. Seeing that most of the students at UiS Subsea have trade certificates in relevant disciplines, meaning various experience from real life application of mechanical systems as well as electrical and software, made the group eager to design and produce an ROV that were more related to a real-life working class ROV such as Oceaneering' Millennium previously shown in Figure 1.2.

## 2.3 Our design

Although there would be clear benefits regarding weight and complexity by using an existing design such as *Ægir* or *Vona*, the challenges presented in the thesis definition would clearly not have been met due to their design being optimized for other tasks. Also, previous ROV's have been designed with other tasks and limitations in mind and so their design will deviate from the requirements of the 2021 competition. UiS Subsea therefore decided to design and construct this year's ROV from scratch, starting off with key capabilities set by the MATE competition as well as the theses definitions.

# 3 Design for assembly

## 3.1 Content in this chapter

- Introduction (to Design for Assembly)
- Producing specifications for a product
- Producing a conceptual design
- Producing a detailed design
- Measurable metrics

## 3.2 Introduction

Design for Assembly (DFA) is a methodology intended to help the designer in the start phase of a project in producing a conceptual design, producing specifications for a product, and producing a detailed design. All of this is to reduce the total amount of parts in the design early in the design phase so the assembly process of a product can be improved, and the cost reduced.

The term cost in this project is measured in the form of fewer parts, fewer processes, less amount of material, cheaper processes et cetera. Although Design for Assembly and Design for Manufacture are commonly referred to as a single methodology, Design for Manufacturing and Assembly (DFMA), each level of a product engages different concepts. These concepts include Design for Assembly (DFA), Design for Quality (DFQ), Design for Manufacture (DFM) and so on, where the most used DFA methodologies are the Boothroyd-Dewhurst (B&D) method, the Lucas method, the Hitachi AEM method, and the modified Westinghouse method. All of these methods improve the assembly process in some way, but none of them assist the designer in all the steps of the process (Ezpeleta, et al., 2019).

Considering the scope of this thesis, it is essential that that the frame of the ROV and the mounting methods that are to hold it all together are efficient and easily modifiable. This is due to the wide amount of external equipment needed for the MATE competition, that will be fitted to the frame. Weight is also a factor that will have to be factored in during the design, production, and assembly phase. Weight can be controlled to an extent during the design of the frame of the ROV, other equipment such as the manipulator arm, the micro-ROV and the electronics container are outside the control of this thesis. The steps taken to ensure DFA during the inception of this ROV was producing specifications for the ROV, producing a conceptual design, and finalizing a detailed design for the first prototype, which is what this ROV is considered to be. By using standardized parts and processes as much as possible, time and cost can be reduced significantly.

There are several benefits in implementing DFA during the conception of a product, such as the time it takes to enter the market, the quality of the end product, manufacturing time, assembly time and part count and cost (Ulrich & Eppinger, 2016).

## 3.3 Producing specifications for a product

During the start phase of UiS Subsea 2021, a brainstorming session with the team was performed to home in on all the details and specifications needed in the MATE competition. A rough idea of how the ROV should look was sketched on a whiteboard. An unspecified number of thrusters were considered, placement of buoyancy, frame structure and manipulator arm placement. All of these ideas would later on serve as a starting point for the conceptual design phase. An eliminating process was performed early on in the development of the product specifications for the ROV, this served to eliminate redundant components and combine functions of two or more into one component, this process can be seen in Figure 3.1. Components were reduced based on complexity and assembly time, and instead of using bolts for individual components, a central way of fitting components to the frame were strived for (Stienstra, u.d.). Material selection was one of the key parameters that was considered early on. Identifying the material properties needed for the ROV to operate, limited the available material to use for production. After choosing suitable materials, the machining process could be chosen. Several discussions on what process to use led to what seemed to be the most efficient ones being chosen for the production of the ROV-frame. Some standardized parts were chosen to limit machining time and cost. Certain manufacturing processes took place inhouse, while others were outsourced due to specialization and machining limitations. The overall design of the ROV incorporated a standardised machining approach. This meant that the machining involved had no need for special tools other than what would be found in a machine shop, or any tolerances needing additional steps. The machining was also planned to have as few operations as possible, limiting the time spent.

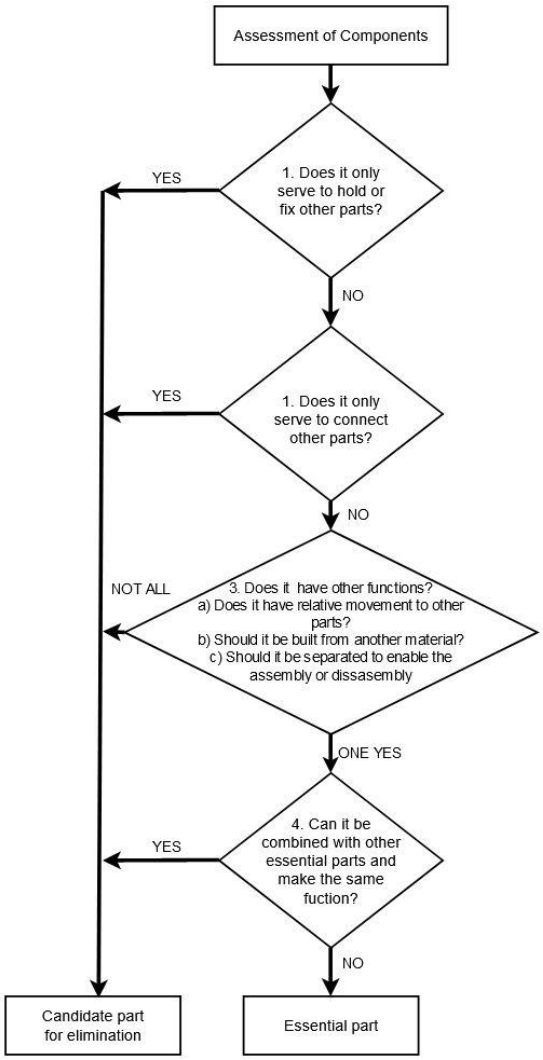


*Figure 3.1 – Elimination process*

The geometry of the parts was also conservative so that no special clamping or machining tools was needed. The geometry of the parts was also chosen to limit stress points that could develop into fractures over time and was designed with the available machines in mind.

## 3.4 Producing a conceptual design

The phase of producing a conceptual design was carried out after the key specifications had been set. Design is a process of creating a solution to a specific problem. The ROV design is based on simplicity, being lightweight, tooling requirement during machining, minimal setups during machining et cetera. The problem at hand was to create an ROV-frame that would have six degrees of freedom to move around in its environment, it would be able to reach a depth of 100 meters, and it should have all its equipment mostly on its inside to protect it from any operational damage. A large amount of the product's life cycle cost stems from determining the early design stages, this means a mass production of this ROV will in all probability result in more revisions (Barton, et al., 2001).

Components designed for the ROV took into account the assembly operations needed to fit them to the ROV, this made the overall assembly fast and efficient. During all the conceptual design phases there was a high focus on addressing costly machining and assembly processes, and to limit these as much as possible. The manufacture and assembly process supplements the product design process, as can be seen in Figure 3.2.

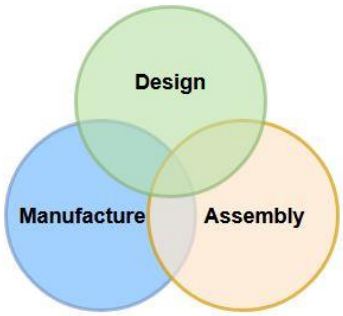


*Figure 3.2 – Design, Manufacture and assembly overlapping each other*

## 3.5 Producing a detailed design

During the finalization of the first ROV design revision, material length was carefully chosen to limit cuts and material loss and thereby reducing potential cost. By using Computer Aided Design (CAD) the design and the fitment of the parts for the ROV could be analysed early in the process, ensuring the most efficient assembly process. Off the shelf components were chosen where possible to limit machining time. Component design were optimized to allow for easy machining, so to limit re-clamping of the components in the machine. An example of component optimization is the thruster mounting brackets that were initially designed to be produced in a series of machining steps. The design of the brackets was later revised to be produced by a single step using a 3-dimensional printer. By altering the manufacturing process during this step, material waste and cost were lowered, and time spent machining could be prioritized more efficiently.

During chapter 4, *Frame design and structure*, a detailed description of the design and thought process will be uncovered. The DFA concept will show through in innovative and efficient solutions applied to the design, manufacture, and assembly process of the ROV.

All of this yielded a first prototype of the ROV ready to accept the electronics, control systems and other equipment produced by the rest of the UiS Subsea team.

## 3.6 Measurable metrics

To get tangible values from the assembly process, certain aspects measured during assembly such as time and calculated cost will be implemented in chapter 4. By inserting these values into equations used in DFA analysis, metrics such as design efficiency, total assembly time and cost, and quality of design can be found.

# 4 Frame design and structure analysis

## 4.1 Content in this chapter

- Introduction (to the frame design and structural analysis)
- Frame design
  - Centre of mass and centre of buoyancy
- Structural analysis
  - Material properties
  - Choice of material
  - Corrosion
- Manufacturing
  - Production methods
  - Fastening alternatives
  - Aluminium welding
  - Additive manufacturing
  - Fused deposition manufacturing
  - Stereolithography
- Assembly
- Conclusion

## 4.2 Introduction

The most important aspect in designing the frame was to consider the overall limitations set by the thesis definition, as well as the rules and regulations given by the MATE competition. Based on these guidelines, aspects such as design, size, weight, thruster positioning et cetera could be determined for the best operational performance. The project was funded by sponsorships provided by local and national companies supporting the subsea industry. Funds would have to be shared across the different disciplines within UiS Subsea equally, this affected the choice of materials and parts. UiS Subsea as a team worked closely together in providing feedback that would contribute to making these design decisions realistic and achievable. An efficient and adaptable frame design would yield a platform suitable to accommodate various equipment in an efficient and compact manner. The design process included using the concept of DFA in all areas of the ROV-frame, this provided a design which was easy to assemble, requiring very little additional time in regard to re-working parts and fitment. In the following chapters, the design process of the frame, the individual parts, and the overall exterior of the ROV will be uncovered.

By using CAD software, a visual representation of the evolving design will be shown. Calculations will back up important decisions made on material choice, fastening methods, welding and so forth.

## 4.3 Frame design

The process of developing the initial ROV design involved several brainstorming sessions where the whole team of UiS Subsea participated. A lot of inspiration was taken from the oil- and gas industry that is associated with Stavanger, the hometown of UiS Subsea. Many great international companies operate on the Norwegian continental shelf, and are based in and around Stavanger, and so inspiration for designing an ROV was taken from industry proven designs and existing products. Traits that would be needed for the MATE competition was stability and compactness, and so the initial idea was to make a frame that would have its buoyancy element placed on top of the ROV, with its centre of weight as low as possible. Furthermore, the ROV would have to be launched from the edge of the competition pool, and so handles would have to be incorporated in an efficient way. Additional equipment during the competition would also be needed, and so the design would correspondingly have to reflect this. To be able to control the ROV efficiently, thruster placement would have to have a high priority, seeing that the effect of thrust would be greatly impacted based on improper placement. Inspiration from existing UiS Subsea, market, and industry ROVs indicated that placing the thrusters far apart from each other would ensure sufficient control authority.

To achieve the required strength and adaptability, it was decided that the frame would incorporate extruded aluminium rails. These rails are a standard of the shelf part, made of a wide variety of alloys, and would ultimately provide a simple yet strong base for attaching supporting frame structures and components. Considering the operational environment, the aluminium would have good properties to resist degradation.

Looking for inspiration in creating an internally strong frame without the need for redundant structures, the focus was directed to the automotive and aircraft industry and the monocoque chassis design. The monocoque, from the Greek word for single (mono) and the French word for shell (coque), is an internal self-bearing construction that differs from the opposite concept of a construction with an internal load-bearing frame often referred to as a chassis (Gudmundsson, 2014).

Choosing the frame to be designed as a monocoque freed up internal space for mounting essential equipment such as thrusters, electronics, manipulator arm et cetera, all while contributing to an overall lower weight. Designs were initially produced on chalk boards and on paper to have a tangible feel, changes were easy to implement, and team members could easily interact with the design. The concept of DFA were relayed to team members that would make their requirements known, and

therefor driving the design forward. Later on, the design was migrated to Autodesk Inventor for visualisation and further modelling which can be seen in the figures below.

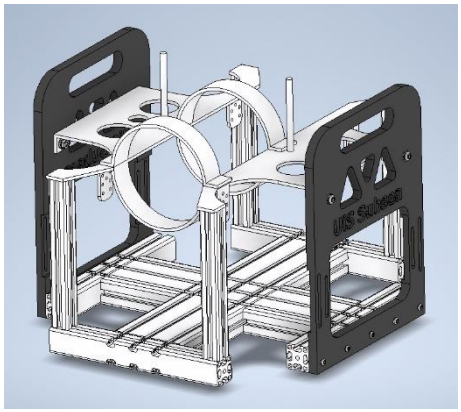

*Figure 4.1 – Monocoque frame design*

The outer design would incorporate the buoyancy element on top of the ROV, with an aluminium frame in the lower part. The lower light grey aluminium frame seen in Figure 4.1 would tie into the buoyancy element by using black side plates. The frame now consisted of a lower part made from light grey machined extruded aluminium rails, connected to black vertical side plates. To tie the side plates together with the lower frame, a mid-plate was designed to combine the electronic container produced by team members in UiS Subsea. This resulted in a compact shell consisting of a lower aluminium frame, tied in with Polyethylene side plates, and connected to the electronic container by an aluminium mid-plate and hoops. Besides the lower part of the frame and the side plates, the mid-plate that ties the lower frame, the side plates and the electronic container together, as can be seen in Figure 4.2, is a crucial part of the frame rigidity.

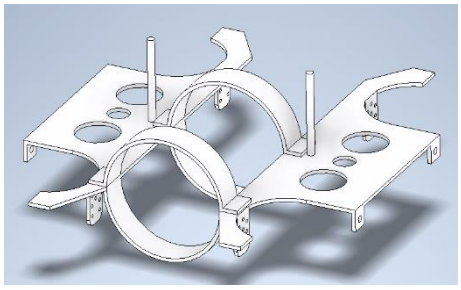
*Figure 4.2 – Mid-plate with aluminium hoops*

When designing the mid-plate and the hoops that ties the electronic container to the frame, the manufacturing and assembly process was prioritized as much as possible. Seeing that the ROV is in a prototype stage, the manufacturing processes of various components are not perfect, they serve to produce a component at the lowest cost and impact of the project, while still having potential for improvement.

The lower part of the frame was initially designed with a certain dimensioned extruded aluminium rail in mind. The outer dimensions of the rail were 120 x 40 mm, and these dimensions served to set the technical specifications for attaching equipment to the ROV, such as the manipulator arm. As the design phase progressed, weight started becoming an issue. Using a full length of extruded 120 x 40 mm aluminium rail in the middle of the lower frame, as seen in Figure 4.3, while also using four 40 x 40 mm extruded aluminium rails at the front and rear as well as side attachment rails, would result in a weight of 7,18 kg. This weight had great potential for improvement

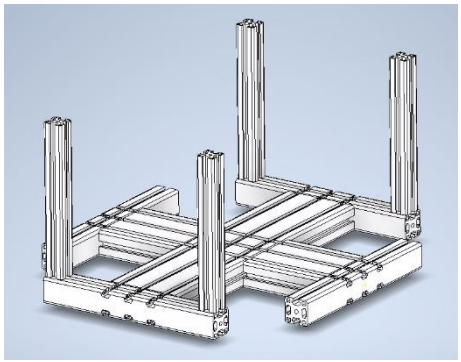
*Figure 4.3 – Lower part of frame, initial design*

and seeing that these extruded rails were standardized off the shelf components the decision to reduce the dimensions from 40 x 40 mm to 30 x 30 mm were taken. The lower frame design now went from having a weight of 7,18 kg to a weight of 3,26 kg, which significantly reduced the overall weight of the frame by 54,6%. Later, also the sections on the side of the lower frame were replaced in favour of hollow 30 x 30 mm box sections to reduce weight even more to a total of 3 kg. These box sections can be seen in Figure 4.4 and 4.5, as the two short longitudinal sections on the side of the frame. The frame went from having a weight of 7,18 kg to 3 kg, this is a reduction of 58,2% and gives added benefits in terms of staying inside the MATE competition weight limitations as well as manoeuvrability.

The final prototype frame design ended up having two full lengths of 30 x 30 mm extruded aluminium rails running the full length of the frame in the X-axis. Two smaller lengths of rail were placed in the front and rear of the longitudinal rails to connect them together. A central piece of rail was fitted with two threaded bars and placed in the middle of the longitudinal rails to ensure two shorter rails being fastened along the Y-axis. To tie the side plates to the lower frame while still being able to keep the weight down, two 30 x 30 mm box sections were placed on the side of the frame. To ensure the box section would not be crushed when fastening the side plate to them, 3D-printed crush preventers was placed inside the box sections, ensuring the weight was kept to a minimum. A crush preventer is shown in Figure 4.5. By 3D-printing the crush preventers, time and weight was saved compared to using full strength extruded aluminium rails, or even machining the crush preventers from aluminium. Doing this ensures the DFA concept is uphold through the design, manufacturing, and assembly process.

*Figure 4.4 – Final prototype frame design*

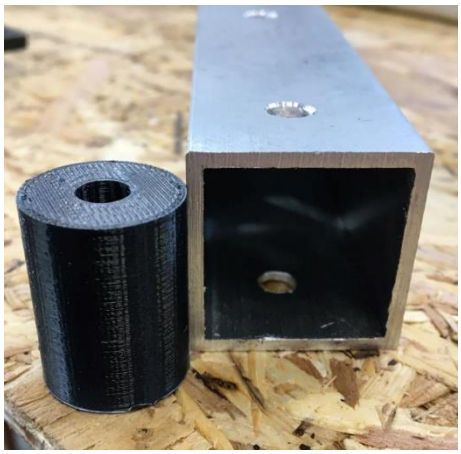

*Figure 4.5 – Crush preventer to be fitted inside 30 x 30 mm box section*

Seeing the ROV would operate in several different configurations, with and without extra equipment, there was a need to be able to adjust the centre of gravity (COG) based on the task and equipment at hand. An innovative way of doing this was to implement adjustment slits in the side plate for mounting the horizontal thrusters. The thrusters have a known weight, and by adjusting them vertically up, or down, it will adjust the COG of the ROV accordingly. By having the thrusters fitted inside the frame, the thrusters contribute to an overall central weight of the ROV, which is desirable for efficient and precise movement.

Fastening of the thrusters to the frame were initially intended to be done by the use of aluminium brackets, welded or bent into the required angle for efficient translative motion. By using DFA, the manufacturing process of four thruster brackets was deemed to take up too many resources in the form of time and material. It was decided, after a stress analysis, that the thruster brackets would be 3D-printed out of ABS plastics instead.

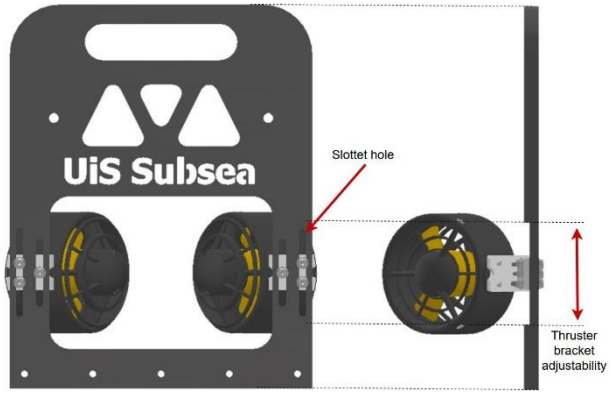


*Figure 4.6 – Front and side view of side plates with two thruster motors fitted. Brackets and thruster adjustability can clearly be seen*

The brackets would be fitted to the side plate on the inside of the frame, as can be seen in Figure 4.6, this resulted in two horizontal thrusters on each side of the ROV that could be easily adjusted to impact the weight distribution, while providing sufficient thrust for translational movement. A way of carrying the ROV were a high priority, and so a carrying handle for an average hand would have to be implemented in the design. Measurements of an average male hand, which is a bit larger than a female one, were recorded and a slotted hole with dimensions of 150 x 35 mm were implemented at the top of the side plates, as seen in Figure 4.6. The plates went through several iterations to make them easily machinable while at the same time have the proper design and function for the task. The manufacturing of the plates was outsourced, and all the cut-outs were machined by using either a water jet or a milling bit with a diameter of 3,5 mm. This is an industry standard size, and limited the need for tool changes, and greatly reduced the time used during manufacturing. The geometry of the side plates included only two clamping procedures, ensuring minimal handling time during manufacturing. These processes do have room for improvement and will in all probability result in change if the ROV will enter mass production. The buoyancy element was initially intended to fit at the top of the ROV ensuring a centre of buoyancy (COB) as high up in the structure as possible. The buoyancy element, although it received several iterations, stayed atop of the ROV. This kept the COB at the top of the ROV, while also making room for equipment internally in the frame. Traditional designs from the industry also mounts the buoyancy element on top of the ROV, for the exact same reasons regarding COB. When it came to the visual design, the large buoyancy element provided an element of vibrancy.

The element was painted in a bright yellow colour as a tribute to the industrial working class ROVs, as well as making the ROV more visible under water. The buoyancy element is a specialty item, and a one-of-a-kind design made from a high-density foam known as HCP30 (Hydraulic Crush Point, measured in Bar). The production of it was therefore outsourced due to this reason, ensuring a high quality of workmanship. The buoyancy foam design would have to incorporate room for the vertical thrusters, the electronic container, allowing for room to place hands through the carrying handle and so on. Adhering to the concept of DFA meant the design would have to be very simple with manufacturing and assembly in mind. Seeing the buoyancy foam would cover the electronics container which is a central part of the operations of the ROV, it was clear that the mounting of it would have to be very efficient and fast. This meant that the buoyancy foam would have to be designed to be self-centring onto the ROV, as well as including an easy way of attaching it to the frame. The final prototype design includes a shape that will align the buoyancy foam with the side plates, this allows it two slip onto two central threaded rods that makes attaching it to the frame as simple as tightening two wing nuts, as can be seen in Figure 4.7. The weight of the ROV is transferred from the threaded rods to the buoyancy foam by two oblong aluminium washers with the dimension of 230 x 40 x 5 mm. By mounting the buoyancy foam like this, time spent on removing it from the ROV is reduced. The design of the buoyancy foam limits machining time and complexity and uses standard machining procedures and tools to make it as simple as possible, this minimizes cost to the project.

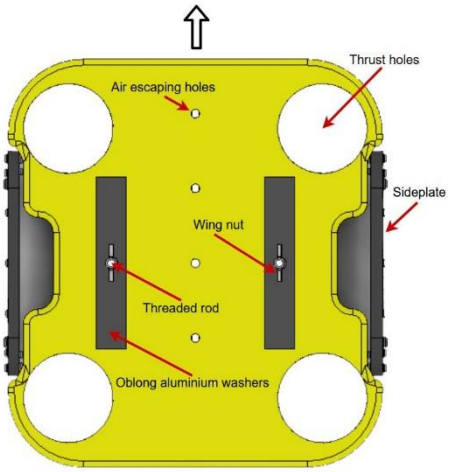


*Figure 4.7 – Top view of ROV showcasing buoyancy foam, oblong aluminium washers and wing nuts*

At this point the ROV had a well-developed overall design consisting of an assembly of as few parts as possible. The ROV had a frame that acted as a load-bearing structure, while still looking attractive and allowing for space to mount equipment. To achieve an efficient hydrodynamic shape that would limit drag when operating under water, covers where designed to fit on each corner of the ROV, tying in the side plates with the extruded aluminium rails in the front and rear. This can be seen in the rendered image of the ROV in Figure 4.8. Several design iterations and manufacturing procedures were considered for the corner covers. The final design ended up being a curved shape with horizontal slotted holes to allow for flow in and around the vertical thrusters. The design of the corner covers was perfect to implement into a 3d-printed manufacturing process. This process was outsourced using the stereolithography method which is covered more in sub-chapter 4.6.6.

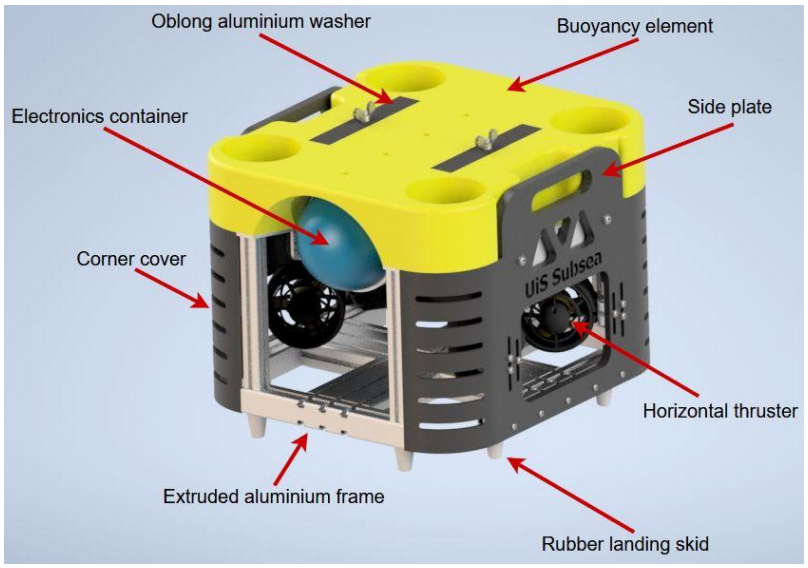


*Figure 4.8 – Rendered image of the prototype ROV, with component names*

## 4.3.1 Centre of mass and centre of buoyancy

It is critical to have a stable manoeuvrability when the ROV is to operate, there are several factors that can affect this. The first is to just slightly have a positive to neutral buoyancy so you do not have to use a lot of power to stand still. And it is desirable to have the COB as high as possible on the overall ROV structure, and the COG as low as possible. this will result in the ROV having good self-correction properties. This makes it easier to operate, and when you stop for any orientation or inspection after driving at an angled surge, the ROV straightens itself without the help of external forces such as thrust. As shown in Figure 4.9, it is desirable to have the longest possible distance between COG and COB, as this will give the greatest self-righting torque around the rotation axis. The locations of these points can be estimated by setting up a table with the centroid coordinates and properties of the various elements and subsystems in a

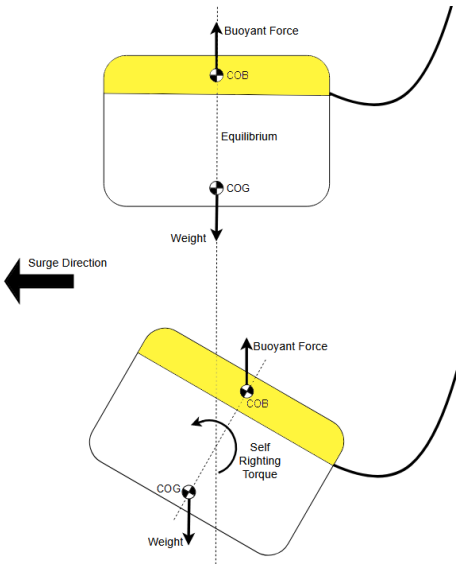


*Figure 4.9 – Graphical visualisation of self-righting torque*

coordinate system as shown in Table 4.1 and utilize these values in equations that solves for COG and COB. In this thesis, this was mainly done through Autodesk Inventor where each component has been given its true material properties for further structural analysis, therefore it is most efficient to use the software to find COB and COG instead of calculations by hand. The achievable optimization of these important properties will be adapted to the time available during this thesis as there are many choices that could make a difference for further development.

*Table 4.1 – Values for calculating centre and magnitude of buoyancy. Values marked with * are close estimates, where (0, 0, 0) has its origin at the bottom rear corner*

| Sub-system | Part(s) | Volume of displaced water ($cm^3$) | Weight of displaced water resulting in Buoyancy force (kg) | Weight of part(s) (kg) | Centroid coordinates (mm) | | | Net Buoyancy force. (N) |
|---|---|---|---|---|---|---|---|---|
| | | | | | X | Y | Z | |
| **Alu. frame** | 4x Vertical beams | 86,25 | 0,09 | 0,93 | 270 | 250 | 155 | -8,24 |
| **Buoyancy** | 1x Main element | 14 153,51 | 14,47 | 2,83 | 270 | 250 | 340 | 114,15 |
| **Mid-plate** | Complete | 577,82 | 0,57 | 1.58 | 270 | 250 | 282 | -9,90 |
| **Side plate** | 2x Side plates | 1886,18 | 1,93 | 1.79 | 270 | 250 | 205 | 1,37 |
| **Electronics** | Container | 6260,17 | 6,33 | 5,20* | 290 | 250 | 282 | 11,08 |
| **Thrust** | 4x Vertical thrusters | 1514,72 | 1,55 | 2,88 | 270 | 250 | 200 | -13,04 |
| **Thrust** | 4x Horizontal thrusters | 1514,72 | 1,55 | 2,88 | 270 | 250 | 100 - 140 | -13,04 |
| **Alu. frame** | All lower horizontal beams (9) | 764,18 | 0,78 | 2,05 | 270 | 250 | 15 | -12,45 |
| **Exterior** | 4x Corner cover | 878,54 | 0,90 | 1,06 | 270 | 250 | 140 | -1,57 |
| **Equipment** | Manipulator arm | 670* | 0.66 | 5,5* | 260 | 250 | 60 | -47,46 |
| **Assembly** | All Nuts, bolts, washers (300-350) | 125* | 0,13* | 0,5* | 270 | 250 | 195 | -3,63 |
| **Other** | | | | | | | | |
| **SUM** | | 26916.37 | 29,75 | 27,2 | | | | 17,61 |

As the ROV must be capable of housing external as well as internal equipment, it is important to maintain a linear vertical relationship between COB and COG to avoid a tilted equilibrium. Therefore, requirements were set for all the teams in UiS Subsea to construct their equipment by placing the heaviest components as close to the centre as possible. Looking at the manipulator arm, it uses a long platform that slides into the extruded aluminium frame, with its motors fitted to it. This allows the heavy motors of the manipulator arm to be placed in the centre of the ROV, and by using axles and drive belts, to transmit the power to the manipulator arm which is relatively lightweight due to its 3D-printed components. Thus, one can use weights placed underneath the ROV's frame to compensate for the smaller weight differences when balancing the ROV in the water.

As of now, the ROV has a theoretical positive buoyancy of 17,6 N. Calculations show that the ROV will have a positive buoyancy where an estimate of 1,7 kg would be necessary to keep it in equilibrium when no thrust is applied. Seeing there are only a few more small components to be implemented such as sonar, LED lights, and a downward looking camera, the buoyancy properties obtained are very satisfactory for an almost neutral or slightly positive buoyancy. These values were considered when the buoyancy element was sent to be manufactured, as the design of the buoyancy element allowed for adjustments in case more or less buoyancy was needed, by removing or adding material. The coordinates of COG and COB are calculated using the values from Table 4.1. An example of calculating COB and COG in the Z-axis is shown in the following equations:

$$Z_{COB} = \frac{\sum_{i=0}^{n} Z_i * Weight\ of\ displaced\ water\ from\ part_i}{Total\ weight\ of\ displaced\ water\ from\ all\ parts}$$

$$Z_{COG} = \frac{\sum_{i=0}^{n} Z_i * Weight\ of\ part_i}{Total\ weight\ of\ parts}$$

As the ROV is approximately symmetrical we can neglect calculating the values in the Y-axis, as this will refer to the centre. By using these equations for the XZ-plane with the values derived we get:

$$X_{COB} = \frac{8157{,}9\ kg*mm}{29{,}75\ kg} = \quad \underline{274.2\ mm}$$

$$Z_{COB} = \frac{8068{,}4\ kg*mm}{29{,}75\ kg} = \quad \underline{271.2\ mm}$$

$$X_{COG} = \frac{7660{,}3\ kg*mm}{27{,}2\ kg} = \qquad \underline{281{,}6\ mm}$$

$$Z_{COG} = \frac{4938{,}3\ kg*mm}{27{,}2\ kg} = \qquad \underline{181.6\ mm}$$

Thus, the ROV has the following coordinates (X, Y, Z) of COB = (274,2 mm. 250,0 mm. 271,2 mm) and COG = (281,6 mm. 250,0 mm. 181,6 mm). With regard to the origin being in the bottom right rear corner, this means that the y-axis goes in the rear edge of the ROV, the x-axis along the right side, and the z-axis starts from the ground plane. Comparing this to the absolute centre of the ROV: (270 mm, 250 mm, 195 mm), the results are deemed satisfactory. If an even greater distance between the points is desired, one can use the remaining available buoyancy force and place weights under the frame to lower the COG even further or balance external equipment. But in all axes the results show that the ROV is well balanced and should have a good self-righting torque that will make it stable and easy to manoeuvre.

## 4.4 Structural analysis

A verification of components that are to be fitted to the ROV is needed to ensure no failures during prototype testing. Having access to powerful computer aided simulations, such as Autodesk Inventor, makes calculating material strengths and properties fast and efficient. There is however a need to make assumptions when analysing components, on the computer and on paper. The assumptions are that the material properties, welds, and bolted connections are ideal, with no structural weaknesses.

To simplify the manufacturing process of the thruster brackets, it was decided to produce them in ABS plastic by using a 3D-printer. Using a 3D-printer in the production of these specialty parts enables a geometry that would otherwise be difficult if not impossible to obtain. To ensure this material would stand up to the task, a simulation of the thruster brackets was performed with all the requirements in place to represent the actual part in operation. Taking the maximum thrust force obtained in chapter 5.5 of 49 N, and simulating a decomposed force of 40,1 N in X- and 28,1 N in the Y-axis yielded a maximum displacement at the red portion of the thruster bracket, shown in Figure 4.10, of 1,792 mm. The displacement will be the same in a negative applied thrust force situation, for example going in reverse. The total deflection will then be the forward and the rearward displacement combined, to a total of approximately 3,6 mm. Using the original thruster bracket dimensions, the angle between the side attaching to the side plate of the ROV,

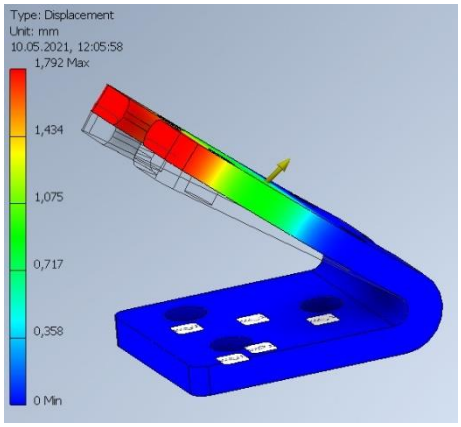


*Figure 4.10 – Maximum displacement of the thruster bracket, shown in red. X-axis along the arrow*

and the side that the thruster attaches to can be calculated. Using the trigonometric relationship of $\sin(\theta) = \frac{O}{H}$, where "$o$" represents the opposite side, and the "$H$" represents the hypotenuse in the triangle formed by the bracket, and solving for θ, one gets:

$$\theta = sin^{-1}\left(\frac{32,7}{57}\right) \approx \underline{35^o}$$

Calculating the angle when a displacement of 1,792 mm occurs yields:

$$\theta = sin^{-1}\left(\frac{34,5}{57}\right) \approx \underline{37,2^o}$$

This is an increase of 2,2° in the positive direction, and a total of 4,4° combined between positive and negative thrust. These values, although unwanted, is deemed to be acceptable for the prototype. Any further development of the ROV would take into account these values and would prioritize development of stronger thruster brackets. Looking at the significance of the thruster brackets as they sit on the ROV, they have more positives in the form of weight savings, complexity during manufacture and so on, than they do negatives. This is the most important thing in terms of moving forward with this design.

The simulations are also performed on the bracket with no bracing fitted, this will allow for more flex at the tip of the bracket than would have been allowed if the bracket were tested with a thruster fitted to it. Simulating the thrust force on the bracket alone will give values based on its material properties, which are relevant for determining its strength capabilities. To confirm that the material strength will be strong enough, a stress analysis using the von Mises hypothesis is performed.

The foundation for this hypothesis is the work $(W)$ done by the deformation on an elastic material, as shown:

$$W = \frac{1}{2}(\sigma_x\varepsilon_x + \sigma_y\varepsilon_y + \sigma_z\varepsilon_z + \tau_{xy}\gamma_{xy} + \tau_{yz}\gamma_{yz} + \tau_{zx}\gamma_{zx})$$

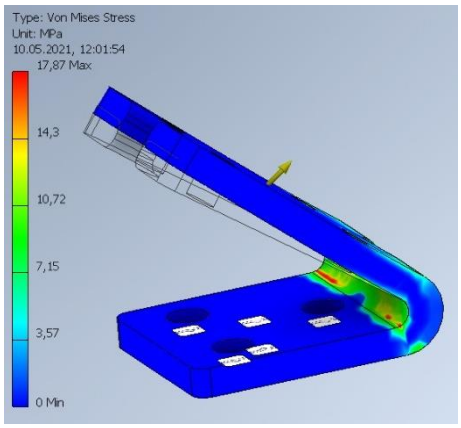


*Figure 4.11 – Maximum von Mises stress at a thrust force of 49 N*

Where $\sigma_i$, $\tau_{ij}$ represents the normal- and shear-stress respectively, and $\varepsilon_i$, $\gamma_{ij}$ represents similar strain components (Lemu, 2020). During simulation of the 3D-printed ABS component, the maximum von Mises stress is calculated to be 17,87 MPa at a thrust force of 49 N. When looking at the yield strength for ABS material, it is the range of 29,6 – 48,0 MPa, this means that during the operation of the ROV with a maximum thrust set at 49 N there should not be any failures due to yield or fracture, as can be seen in Figure 4.11.

Seeing there is a safety factor of $\frac{29,6}{17,87} \approx \underline{1,66}$, the material is strong enough for the application. If the thruster where to be operated at the maximum thrust available at 192 watts, as calculated in chapter 5.5, the simulations show a maximum von Mises stress calculated at 21,18 MPa. Computing the safety factor for the potential increased thrust force of 58 N, gives $\frac{29,6}{21,18} \approx \underline{1,39}$, which indicates that at the lowest yield strength of ABS, the material is still not at risk of failure due to yield or fracture. This is important to know in the proceeding development of the ROV. 3D-printing the thruster brackets of a material with a higher yield strength, or to investigate other materials and manufacturing processes could be beneficial in reducing flex all together.

The mid-plate connecting the lower part of the aluminium frame to the side plates and the electrical container, included welding. It was therefore important to know the strength capabilities of the welds regarding the rest of the mechanical connections. The weld connections were covered by manual calculations as well as computational simulations to ensure a component free for any failures during testing. The simulations show a maximum displacement of 0,09413 mm when the thrusters are running at full load conditions, this can be seen in Figure 4.12. The thrusters are acting against the positive buoyancy generated by the buoyancy element, and with a maximum material displacement of just slightly more than a human hair, it is considered negligible. What is more important for the prototype testing is the von Mises stress analysis compared to the material properties. The analysis takes into consideration the welds laid at the lower parts of the aluminium hoops, as well as the minimum yield strength of Aluminium 6061-T6 of 240 MPa.

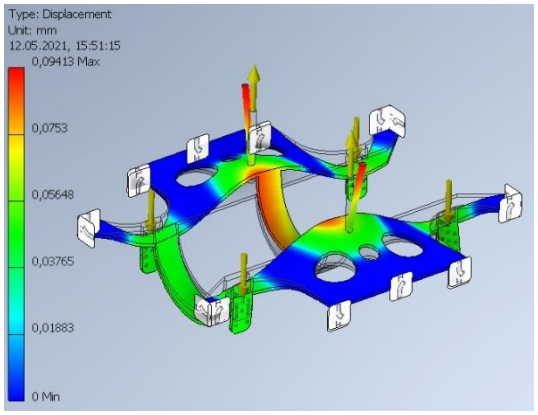


*Figure 4.12 – Maximum displacement of the mid-plate during full load conditions*

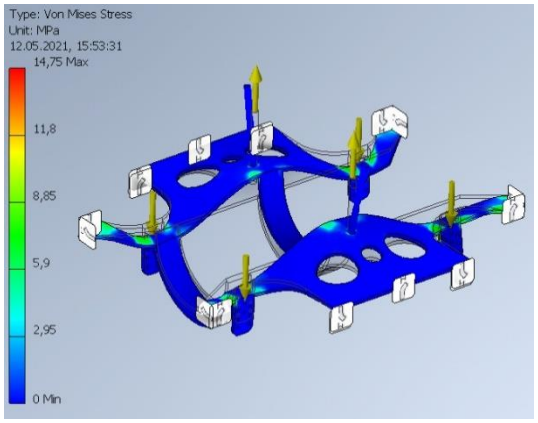


*Figure 4.13 – Maximum von Mises stress during full load conditions*

The maximum von Mises stress found during the computational simulations peaked at 14,75 MPa, as seen in Figure 4.13. Comparing this value to the tensile yield strength for 6061-T6 aluminium, it is clear that the aluminium structure will have no problem handling the forces during operation. There is a calculated safety factor of $\frac{240}{14,75} \approx \underline{16,27}$, which suggest that upon further development of the ROV prototype, the thickness of the aluminium mid-plate could be decreased significantly. Doing this could help reduce weight, cost of machining, and material cost.

The relevant forces applied to the welds are mainly the weight of the electronics container. This is estimated to be 5,2 kg which will apply a force of 51 N distributed over two hoops, where each hoop has a structural fillet weld at each end. This means that each weld is exposed to a static load of approximately 12,75 N. In reality, it will be exposed to a higher force if the ROV is carelessly lowered to the ground. Therefore, calculations will take into account an arbitrary force of 50 N on each weld, giving them an approximate safety factor of almost $\frac{50}{12,75} \approx \underline{4}$. This also simplifies the calculations on the thruster brackets. In chapter 5.5, it is deduced that the maximum thrust force is 49 N from each individual thruster. Thus, all conditions are identical, with the same material, material thickness, welding type and welding dimensions.

Seeing that aluminium 6061-T6, has a yield strength of 240 MPa, and that the welds are manually performed, the effective a-measure is simply the thickness from the welding root corner to the surface. A thickness of t = 8 mm was measured after the fillet weld was applied. Thus, the weld's throat thickness (a) is:

$$a = t_w * \text{Cos } 45^o = \underline{\text{5,7 mm}}$$

A safety factor of at least $n_w$ = 1,5 on the calculations is desired. This is in addition to the safety precautions already set in the aluminium hoops. Therefore, the acceptable stress is:

$$\sigma_{allowed} = \frac{\sigma_{failure}}{n_w} = \frac{240\ MPa}{1,5} = \underline{\text{160 MPa}}$$

It was then important to find the $A_{section}$ of the weld, which accounts for the throat thickness combined with the weld length. This gives the following:

$$A_{section} = a * L = 5,7\ mm * 40\ mm = \underline{\text{228 mm}^2}$$

Thus, the nominal axial stress on each weld is:

$$\sigma = \frac{F}{2 * A_{Section}} = \frac{50\ N}{2 * 228\ mm^2} = \underline{\text{0,11 MPa}}$$

Symmetry on the hoops gives:

$$\tau_{\perp} = \sigma_{\perp} = \sigma * \text{Cos } 45^o = \underline{\text{0,08 MPa}}$$

Which results in an equivalent stress of:

$$\sigma_{equivalent} = \sqrt{{\sigma_{\perp}}^2 + 3 * {\tau_{\perp}}^2} = \sqrt{(0.08\ \text{MPa})^2 + 3 * (0.08\ \text{MPa})^2} = \underline{0{,}16\ \text{MPa}}$$

It was concluded that the safety factor is so astronomical that if this specific part were to be mass-produced, material saving measures could have been taken for cheaper production while still maintaining enough strength. As seen in Figure 4.14 (a) and (b), a bending moment is also applied to the thruster bracket because of the force being applied at a greater distance from the weld measurements.

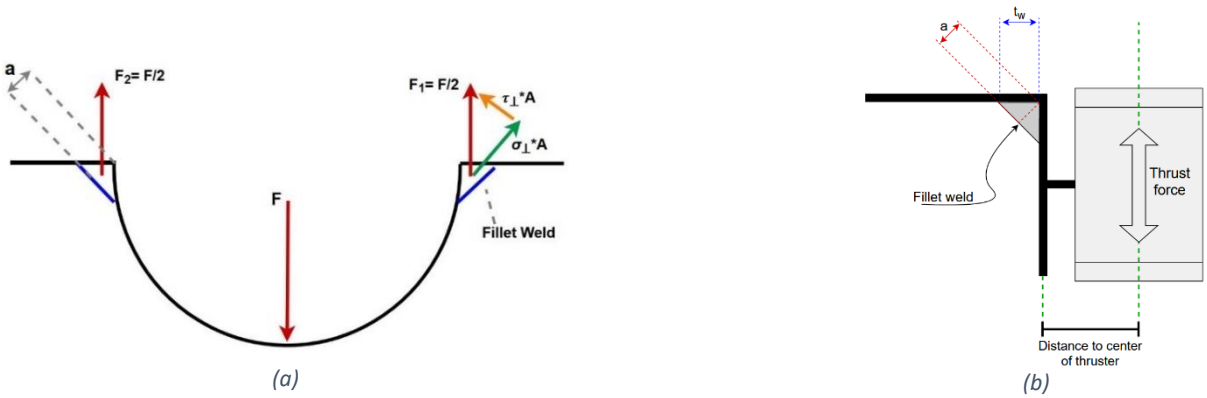


*Figure 4.14 – Overview of forces decomposed on the lower aluminium hoops, and thruster bending moment. (a) Forces on the lower hoops and welds, while (b) Thruster bending moment on welds*

The distance to the centre of the thruster is 73 mm. Therefore, we have the bending moment and resistance:

$$M_b = Thrustforce * Distance\ to\ center\ of\ thruster = 50\ N * 73\ mm = \underline{3650\ \text{Nmm}}$$

$$W_b = \frac{L*(Distance\ to\ center\ of\ thruster)^2}{6} = \frac{40\ mm*(73\ mm)^2}{6} = \underline{35527\ \text{mm}^3}$$

$$\sigma_{bending} = \frac{M_b}{W_b} = \frac{3650\ Nmm}{35527\ mm^3} = \underline{0{,}10\ \text{MPa}}$$

It is concluded that none of the welds are in any danger of failure due to yield.

The centre beams are subjected to a torque which it has to withstand and is where the rear screws on the manipulator platform are attached to the frame. This takes into account a pivot point at the front end of the ROV where the manipulator platform distributes the load on a transverse beam, so this will result in an upward pulling force as the manipulator performs a lift. This lift is set to 5 N, and performed at the maximum distance of 50 cm extended from the frame, this results in a force in the centre of:

$$M_{Centre\ beam} = 5\ N * 0{,}5\ m - F * \frac{0{,}54\ m}{2} = 0$$

$$F \approx 9{,}26\ N$$

Seeing that the force is distributed over 2 beams, each beam is subjected to a force of:

$$\frac{9{,}26\ N}{2} = \underline{4{,}63\ N}$$

As seen in Figure 4.15 (a) and (b), this will only inflict a displacement of $\underline{6{,}28 * 10^{-4}\ mm}$, and a maximum Von Mises Stress of <u>0,08 MPa</u>, and is concluded to have an insignificant stress load.

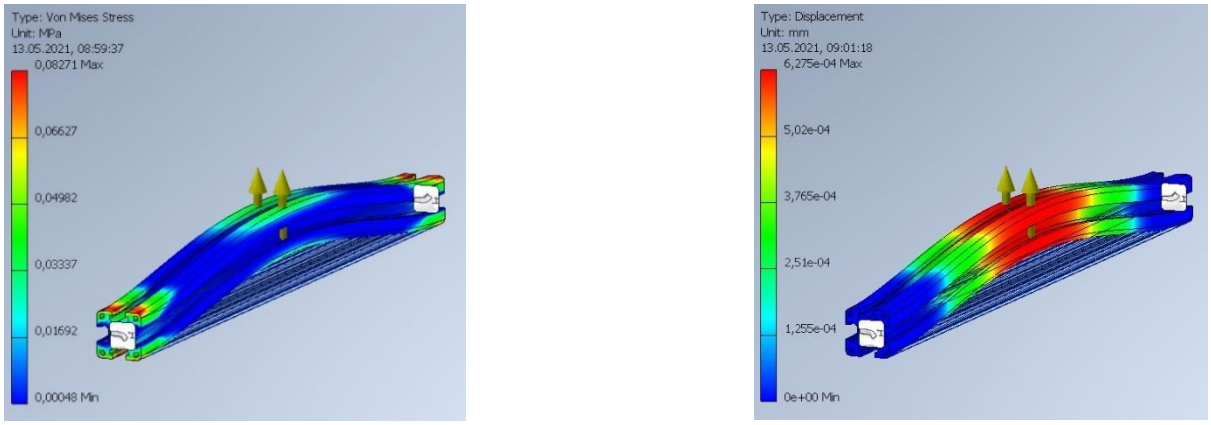


*(a)* *(b)*

*Figure 4.15 – Forces of bending moment applied to the lower frame beams running in the X-axis, as shown in Figure 5.1. (a) Maximum von Mises stress, and (b) Maximum displacement*

During the entire assembly, only acid proof stainless-steel grade screws, nuts, and washers of the quality A4-70 were used. These have excellent corrosion resistance, and for calculations the following properties will be applied. A minimum tensile strength of 700 MPa, yield strength ($R_e$) of 450 MPa and Young's modulus (E) of 193 GPa. M6 screws are mainly used, these have a thread pitch of 1 mm, and a threaded bolt stress area ($A_s$) of 20,12 mm$^2$, and non-threaded area (A) of 28,27 mm$^2$. It is desired to fasten the screws up to 70% of the yield strength, this is to not over-tighten since some of the materials are softer, such as the side plates that consist of PE-plastic. The bolts for the side plate go through an aluminium box section of 30 mm thickness, the thickness of the side plate of 15 mm. Therefore, bolts with a total length ($L_{total}$) of 60mm were chosen, where 40 mm is non threaded. See Figure 4.16.

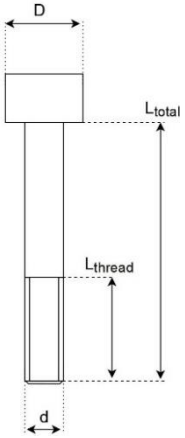

*Figure 4.16 - Bolt*

Thus, we can first calculate the stiffness of the bolt, and then the deformation caused by tightening. threaded length, bolt stiffness ($k_{thread}$):

$$k_{thread} = \frac{A_s * E}{L_{total} - L_{non-threaded}} = \frac{20{,}12\ mm^2 * 193000\ MPa}{60\ mm - 40\ mm} = \underline{194158\ N/mm}$$

non-threaded, bolt stiffness:

$$k_{non-threaded} = \frac{A * E}{L_{total} - L_{thread}} = \frac{28{,}27\ mm^2 * 193000\ MPa}{60\ mm - 20\ mm} = \underline{135402{,}75\ N/mm}$$

This gives a total bolt stiffness ($k_{total}$) of:

$$k_{total} = \frac{k_{thread} * k_{non-threaded}}{k_{thread} + k_{non-threaded}} = \frac{194158\ \frac{N}{mm} * 135402{,}75\ \frac{N}{mm}}{194158\ \frac{N}{mm} + 135402{,}75\ \frac{N}{mm}} = \underline{79771{,}41\ N/mm}$$

This information can be used to find the elongation that the screw achieves when tightened to the desired percentage of the yield strength, in this case 70%. The connection force (F), which can be seen as a force that runs linearly through the axis of the bolt, clamping the objects together will be:

$$\mathrm{F} = 0{,}70 * R_e * A_s = 0{,}70 * 450\ MPa * 20{,}12\ mm^2 = 6337{,}80\ \mathrm{N} \approx \underline{6{,}34\ \mathrm{kN}}$$

The elongation of the bolts will be:

$$\delta_{bolt} = \frac{F}{k_{total}} = \frac{6337{,}80\ N}{79771{,}41\frac{N}{mm}} = 0{,}079\ \text{mm} \approx \underline{0{,}08\ \text{mm}}$$

When all these values are known, it can be used to calculate the deformation of the elements being tightened. This is done with the following formulas:

Stiffness of element ($k_{element}$) formula, where (D) is diameter of the bolt/nut surface on the element. $E_{element}$ represent the Young's modulus of the specific material the element is made of.

$$k_{element} = \frac{\pi * \left(D^2 - {d_{hole}}^2\right)}{4} * \frac{E_{element}}{L_{total}}$$

Then the deformation on the specific element is:

$$\delta_{element} = \frac{F}{k_{element}}$$

A calculation on aluminium 6060-T6 will be derived, based on the bolt conditions above for the sake of simplicity, as well as the part being seen as a solid block of aluminium. The results of deformation will give a clear indication on why washers have been used through the assembly process. The M6 bolts and nuts used has a head diameter of 10 mm, and washers used have a diameter of 17 mm.

Deformation without washers:

$$\delta_{without\ washers} = \frac{6337{,}80\ N}{\frac{\pi*((10\ mm)^2-(6{,}5\ mm)^2)}{4}*\frac{69\,000\ MPa}{60\ mm}} = \underline{0{,}122\ \text{mm}}$$

Deformation with washers:

$$\delta_{washers} = \frac{6337{,}80\ N}{\frac{\pi*((17\ mm)^2-(6{,}5\ mm)^2)}{4}*\frac{69\,000\ MPa}{60\ mm}} = \underline{0{,}028\ \text{mm}}$$

Thus, it can be concluded that in the calculation case, there is a significant potential to avoid deformation by using washers. This backs up why washers were used throughout the assembly process.

### 4.4.1 Material properties

When considering the correct material for a certain task, it is important to know its mechanical properties. The mechanical properties related to a certain metal or alloy have been ascertained by performing laboratory test designed to simulate the materials operational conditions (Callister, Jr. & Rethwisch, 2014). Important mechanical properties of high importance are stiffness, strength, hardness, ductility, and toughness, and Poisson's ratio where:

- *Stiffness* is an indication on a materials ability to return to its original shape after an applied load has been removed.
- *Strength* is an indication on a materials ability to withstand an applied load without failure or plastic deformation (deformation where a permanent distortion has occurred).
- *Hardness* is an indication on a materials ability to withstand localized plastic deformation caused either by a mechanical indentation or abrasion.
- *Ductility* is the ability for a material to withstand a large permanent deformation, such as being stretched plastically without fracturing.
- *Toughness* is a materials ability to absorb energy and withstand shocks that could lead to fracture.
- *Poisson's ratio* is the deformation of the material perpendicular to the direction of the applied force.

An important test factor is *engineering stress* or just *stress*, denoted by the lowercase Greek letter sigma, σ. Engineering stress is given by: $\sigma = \frac{F}{A_0}$, where F is the force applied and $A_0$ is the original cross-sectional area before any load is applied, where the units are given in megapascals, MPa.

Another important test factor is *engineering strain* or just *strain*, denoted by the lowercase Greek letter epsilon, ε. Engineering strain is given by: $\varepsilon = \frac{l_i - l_0}{l_0} = \frac{\Delta l}{l_0}$, where $l_0$ is the original length, and $\Delta l$ is the deformational elongation of a material at some instant. Strain is unitless.

These test values are often combined in a computer program to represent the elongation of a material based on the applied load. The testing is performed in a tensile test machine, with the material machined to a standardized shape. Materials tested at relatively low levels of strain and stress will be proportional to each other by the relationship known as Hooke's law, and where the constant of proportionality *E* is known as the modulus of elasticity, or Young's modulus:

$$\sigma = E\varepsilon$$

Young's modulus is determined as the slope of the material characteristic during testing:

$$Young's\ modulus = \frac{rise}{run} = \frac{\sigma}{\varepsilon}$$

When testing a material, it may be beneficial to test its true stress compared to engineering stress. The benefits of testing one over the other is due to the cross-sectional area that is becoming smaller as the test specimen is being plastically deformed. By using engineering stress, the initial cross-sectional area is used as a fixed value, indicating that the material is becoming weaker when in fact it is becoming stronger due to strain hardening caused by dislocations in the materials crystalline structure. As the real area $A_0$ is becoming smaller the measured stress is becoming larger, indicating a weakening material. By using true stress, the instantaneous cross-sectional area is used when calculating the stress. The equation used to measure true stress is similar to engineering stress:

$$\sigma_T = \frac{F}{A_i}$$

The difference between engineering stress and true stress lays in the measure of the cross-sectional area, and although true stress represents a more accurate measurement, it is also harder to measure.

Another important material property is Poisson's ratio, denoted by the lowercase Greek letter nu, ν. Poisson's ratio is defined by the ratio between the lateral and axial strains:

$$\nu = -\frac{\varepsilon_x}{\varepsilon_z} = -\frac{\varepsilon_y}{\varepsilon_z}$$

Where $\varepsilon_x$ and $\varepsilon_y$ represent compressive strain. If tensile stress is induced on a metal specimen, there will be an elongation and consequent strain $\varepsilon_z$ as a result in the direction of the applied stress. If a uniaxial stress is applied on a material that is isotropic, then $\varepsilon_x = \varepsilon_y$.

In Figure 4.17 one can see the stress-strain curve between engineering stress and strain, and true stress and strain. Here one can clearly see how the material properties seems to weaken as strain increases (blue graph), while the opposite is in fact true (red graph).

All of the abovementioned material properties was considered when selecting materials, this was done when setting the specification of the ROV and during the conceptual design phase. Material choices are covered more in depth in sub-chapter 4.4.2.

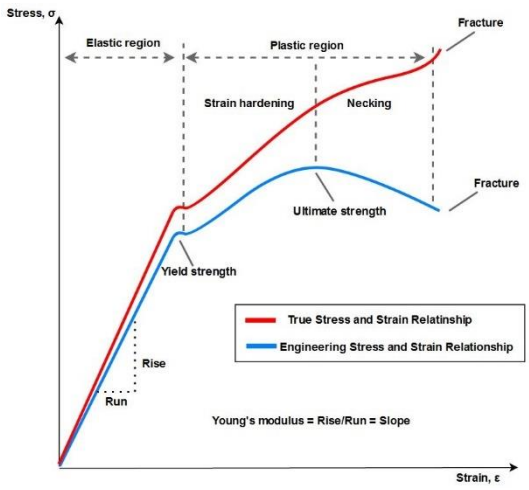


*Figure 4.17 – Stress-strain curve. Showing engineering, and true stress and strain*

### 4.4.2 Choice of materials

Material choice were made based on a requirement of low weight, corrosion resistance and the ease of machining during production. The design was set to have an internal lower frame that thrusters, as well as side-plates and vertical tie-in beams would affix to, and then a mid-plate that would support an electronics container. The overall construction of the ROV would be based upon a design found within the automotive industry, referred to as a unibody. Basing the design of the ROV around the concept of a unibody would provide a structure that would act as a chassis and bodywork all in one. This would result in a lower part count, easier assembly, and an overall pleasing design.

The thesis definition did not set any limitations on the environment of which the ROV is to operate in, however, the MATE Competition rules and regulations states that the competition environment will be in an indoor swimming pool, with chlorinated water, at a depth of up to 7 meters. During the design phase the UiS Subsea team agreed to set one design parameter fairly high, and that was to ensure the ROV could operate down to a theoretical depth of 100 meters. The overall design would have to accommodate this, as well as taking into consideration the seawater effects on the vehicle.

Polyoxymethylene (POM) was due to its high strength, hardness and rigidity considered as side plates on the ROV. Later the material was altered to Polyethylene (PE) which is lighter, but still durable enough for the applications needed in this project. PE also has the added benefit of having a density lower than water, which makes it float.

The main frame consists of aluminium extrusions made of the aluminium alloy 6063 which is suitable for modest strength properties and applications. The main strength requirements are based on the ability to support the weight of the ROV with equipment attached and being able to manoeuvre accordingly. Calculations that are made to support the choice of materials, can be seen in chapter 4.4, structural analysis. Relevant material properties used or discussed during this thesis is shown in Table 4.2.

*Table 4.2 – Material properties for relevant materials discussed during this thesis (MatWeb - Material Property Data, 2021)*

| ***Material*** | ***Material composition*** | ***Young's Modulus (GPa)*** | ***Yield strength ($R_e$) (MPa)*** | ***Tensile strength (MPa)*** | ***Poisson's ratio, ν*** | ***Density, ρ ($g/cm^3$)*** |
|---|---|---|---|---|---|---|
| **POM** | Polyoxymethylene | 2,6 – 3,2 | 67 | 69 | 0,37 | 1,39 – 1,42 |
| **PE** | Polyethylene | 0,3 | 23 – 29,5 | 15,2 – 45 | 0,46 | 0,975 |
| **ABS** | Styrene, acrylonitrile, polybutadiene | 1,19 – 2,90 | 13 – 65 | 22,1 – 74 | 0,29 | 1,05 |
| **Glass filled Polyurethane** | Polycarbamate | 0,621 – 5,5 | 52,4 – 79,3 | 28 – 96 | 0,48 – 0,5 | 1,28 – 1,66 |
| **6063** | 0.7% Mg, 0.4% Si, 98.9% Al | 68,3 | 120 – 190 | 190 | 0,33 | 2,69 |
| **6061-T6** | 97.9% Al, 0.6% Si, 1.0% Mg, 0.2% Cr, 0.28% Cu | 69 | 241 | 290 | 0,33 | 2,70 |
| **A4-70** | 0,08% C, 1% Si, 2% Mn, 0,05% P, 0,03% S, 16-18,5% Cr, 2-3% Mo, 10-14,4% Ni | 193 | 450 | 700 | 0,27–0,30 | 8 |
| **HCP30** | Polyvinyl chloride | 0,31 | N/A | 7,1 | N/A | 0,18–0,23 |

### 4.4.3 Corrosion

The environmental conditions the ROV will operate in are highly corrosive to unsuitable materials. Much consideration is therefore taken to ensure longevity and performance of the ROV. Corrosion is defined as the destructive and unintentional degradation of a metal. It is electrochemical, and often begins at the surface. Combining two materials may cause one or the other to suffer as an anode, the metal then loses or gives up electrons in what is called oxidation which is the area at which the corrosion takes place. Corrosion happens mainly on metals, whereas oxidation can happen everywhere. The combination of materials is important due to this factor, and assembly methods for the frame and adjoining components are closely considered because of it.

There are several forms of corrosion to be considered for this project. One of the more prominent ones applicable for the ROV is galvanic corrosion which could occur between two metals or alloys mechanically joined while exposed to an electrolyte, in this case seawater. There are many solutions taken to hinder oxidation and galvanic corrosion on the ROV, one of them being the possible use of a sacrificial material such as a zinc anode. Zink anodes are commonly used in maritime environments, and work by having a more negative electrochemical potential than its surrounding materials, effectively being consumed in place of the material it is protecting (Chemistry LibreTexts, 2020).

Some parts of the frame have been welded, and there are possible internal stresses imposed on the material that could affect the joint, making it more susceptible for oxidation or galvanic corrosion. Solutions for preventing corrosion at these weld areas are to use zinc anodes as previously mentioned, or by coating them in clear lacquer, preventing the welds having physical contact with the environment at the welded area.

In areas where A4-70 acid proof stainless-steel grade bolts have been used to connect aluminium frame components together, a silicone lubricant has been applied. The reasoning behind this is to isolate the A4-70 acid proof stainless-steel grade bolts from the aluminium to prevent any potential corrosion (Marsh Fasteners, 2020). This is an experiment that would have to be monitored over time, and during further development, approved upon.

## 4.5 Manufacturing

UiS Subsea aims to compete in the 2021 MATE competition, to do this the team will need a physical product that is envisioned, designed, manufactured, and tested. Although this thesis revolves around the theoretical implementation of the concept DFA, and analysis of the thrusters, a final physical product has also been designed, manufactured, and assembled. The final product is the 2021 UiS Subsea ROV prototype, consisting of the outer frame that will allow for attaching thrusters, electronic containers, connectors, manipulator arm and so on. The frame has been manufactured in-house at the University of Stavanger, were milling of a part of the frame can be seen in Figure 4.18, with only a few parts being outsourced to specialists. The hand-over date to finalize the ROV was April 1st, this allowed the electrical teams to implement their equipment into the frame, while receiving support if needed.

*Figure 4.18 – Milling parts of the ROV-frame at the University of Stavanger*

### 4.5.1 Production methods

During the conceptual design phase, it became clear that a combination of using the milling machine, the lathe and so on would be needed. The University of Stavanger has an extensive workshop, enabling the manufacturing of most of the components needed for this project. The mid-plate involved the use of TIG welding and is covered in more detail in sub-chapter 4.5.3. Other manufacturing processes included the use of 3D-printers, which is covered in detail in sub-chapter 4.5.4 – 4.5.6.

### 4.5.2 Fastening alternatives

The construction of the ROV-frame needed to implement connections using bolts, nuts, and washers. When setting specifications, and during the conceptual design phase, standardized fastening components was considered to limit component complexity. Also, by limiting the selection of components, time sorting bolts, nuts, and washers during assembly could be minimized.

It was clear that the mid-plate, shown in Figure 4.2, would be the most complex part of the ROV based on how it would have to be manufactured and how many tie-in points it would have. Several iterations on how to attach all needed components to the mid-plate were discussed. The finalized mid-plate prototype design, as can be seen fitted to the ROV-frame in Figure 4.19, included aluminium Tungsten Inert Gas (TIG) welding. In the mid-plate design, twelve separate components were joined using TIG welding. Seeing the complexity of the mid-plate design, TIG welding was the option that was considered to be the most efficient when taking into account time and manufacturing cost. With more time to spend, the mid-plate is a central part to re-visit and to make more efficient manufacturing wise. When it comes to assembly, the mid-plate truly shines. It has four attaching points that connects it to the side plates and to the lower aluminium plate, ensuring structural rigidity through the two lower aluminium hoops that can be seen in Figure 4.19, even when the electronic container is not present.

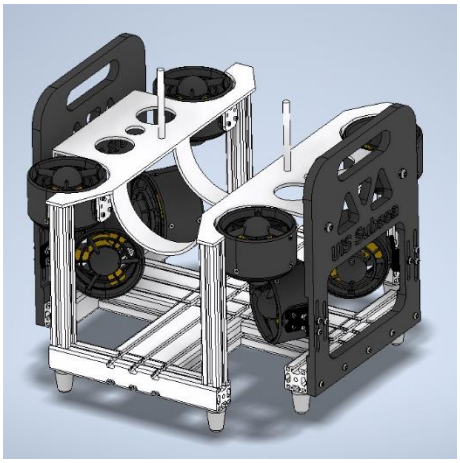

*Figure 4.19 – Front view of the ROV-frame. Lower aluminium hoops seen in the centre of the ROV-frame*

### 4.5.3 Aluminium welding

During the manufacturing of the mid-plate, the TIG welding method was implemented. TIG welding, also known as heliarc welding when used in combination with Helium [He] shielding gas, uses a tungsten electrode that can be used with or without a filler rod. The filler rod must be made of the same material that you are welding and works by melting and joining two metal pieces together, as can be seen in Figure 4.20. Welding aluminium is a very clean process in which an alternating current (AC) pulse provided by the TIG welding machine breaks down a tenacious surface oxide layer formed on the surface of the aluminium itself, while shielding the melting pool with an inert gas, usually Argon [Ar], Helium [He] or Carbon Dioxide [$CO_2$] (The Open University, 2018). The TIG process leaves little to no slag, which is a by-product caused by impurities within the melting pool that solidifies on top of the weld, reducing the post-cleaning operations.

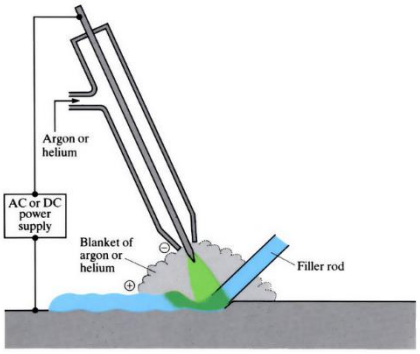


*Figure 4.20 – Principles of TIG welding (The Open University, 2018)*

The welding machine used for welding the mid-plate is a Lincoln Electric Square Wave TIG 255. The machine was capable of continuous welding aluminium of up to 5 mm thickness at 255 amps, with a peak value of 6,3 mm at 305 amps, which was more than enough for welding the 5 mm plates and aluminium hoops together, as can be seen in Figure 4.21. Before welding, the materials were preheated, this was done to reduce the risk of weld cracking that could occur when welding under less-than-ideal conditions (Lincoln Electric, 2021).

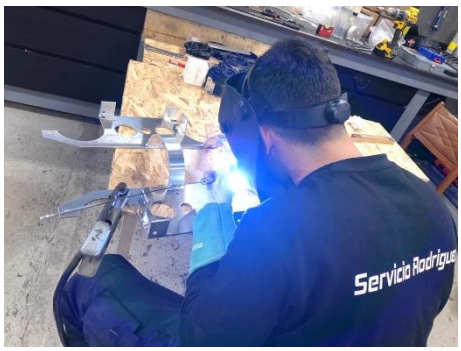


*Figure 4.21 – TIG welding aluminium brackets and hoops to mid-plate*

The aluminium used in the mid-plate, hoops and oblong washers is the alloy 6060-T6. This alloy is very widely used in the conventional industry since it has good structural, machining and weldability properties, and is also relatively inexpensive if one is to lower the production costs. The mid-plate is welded together by two hoops that will curve under the electronics container. At the same time, it has welded on four thruster brackets that hold the vertical thrusters. These welded parts are made from a flat bar of aluminium that is 5 mm thick and 40 mm wide, so the same thickness as the mid-plate. This will make the weld joints more reliable as the parts need the same settings on the welding machine. The type of weld performed, is called a fillet weld, and is often used where the strength requirements are moderate (Härkegård, 2004).

### 4.5.4 Additive manufacturing

Additive manufacturing or 3-dimensional (3D) printing as it has come to be known is nothing new, the technology has existed in various shapes and forms in the amateur and professional market for several years all the way back to 1984. The concept builds upon the idea of using a liquid or a solid material and then solidifying this material in intricate shapes and figures. The use for this technology seems to have no boundaries, being implemented in private homes, medical laboratories, and everything in between. The first patented 3D printer was created by Charles W. Hull, an American engineer, and used a technology called stereolithography (SLA) where liquid photopolymers were hardened using ultraviolet light, creating shapes and figures. Hull has later become known as the father of 3D printing (Gokhare, et al., 2017).

### 4.5.5 Fused Deposition Manufacturing

During the design phase, several parts were designed and then re-designed bearing in mind the manufacturing process. Intricate parts with sharp bends were originally intended to be manufactured by machining and welding aluminium, these were instead 3D printed in strong polymer materials by the use of Fused Deposition Manufacturing (FDM), which is a printing method where a string of polymer material (filament) with a thickness ranging from 1,75 – 2,85 mm is melted through a heated nozzle and then distributed against a flat heated bed. The movement of the nozzle, the temperature of both the nozzle and heated bed and the filament extrusion rate are all controlled by a geometric code (g-code). The g-code is produced by a computer program referred to as a slicer. The slicer program takes a 3-dimensional design produced in a CAD software, and then splits the design into layers depending on how the FDM printer will produce the part, this can be seen in Figure 4.22.

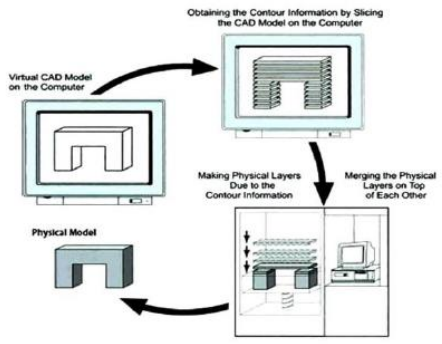


*Figure 4.22 – Graphical representation of a slicer program*

Variables such as the infill of the part, support material and so on can be adjusted to suit the part needed. During the manufacturing process, the ROV received four 3D-printed 35° horizontal motor mounts printed with 100% infill, meaning the parts were solid with no free volume inside. Printing this way also ensures that the parts are very strong. The mounts were originally intended to be produced either by bending an aluminium bar, or by machining a solid block of aluminium. By producing these parts using a FDM printer, time could be spent doing other work on the ROV (Gokhare, et al., 2017). The thruster brackets were tested and found to be strong enough, as can be seen in chapter 4.4, structural analysis.

### 4.5.6 Stereolithography

UiS Subsea collaborated with Mechman AS, a local subsea buoyancy producer located at Jørpeland just outside of Stavanger. Mechman would produce the buoyancy foam needed to keep the ROV afloat in water, as well as any covers or details needed. To protect the internals of the ROV as well as to give it a uniform look, covers were designed to be fitted on each corner. These covers were printed using the stereolithography (SLA) method which is a method that uses a liquid solution made up of photopolymers that harden when exposed to ultraviolet light. The printer was a Photocentric LC Magna with a 510 x 280 x 350 mm build volume (Photocentric, 2021). Photopolymers, often referred to as resin, is poured into a container within the SLA printer. A horizontally flipped print bed is lowered into the resin, where at the bottom of the container a Liquid Crystal Display (LCD) shines UV light at the print bed, solidifying the resin between the LCD and the print bed itself. This process relies heavily on the resolution of the LCD in its ability to create high resolution parts. SLA printers are able to deliver print quality previously impossible by the use of traditional manufacturing techniques. Mechman is currently looking to expand its market presence within SLA manufacturing, UiS Subsea integrates this process well in its ROV design by using the SLA printed corner covers.

## 4.6 Assembly

The ROV was manufactured and assembled during one work week, a total of 40 hours. The DFA concept that was implemented from the beginning really shined through during manufacturing and assembly. All the 3D-printed parts were being manufactured during the machining of the extruded aluminium rails; this increased the overall production efficiency. All the components that would be used during assembly were manufactured in the course of two full days, a total of 16 hours. The specialty parts that where outsourced had a lead time ranging from a few days to several weeks. This was taken into account and planned for prior to the assembly process. Good planning during the design phase ensured components that had a very good fit and made the assembly process fast and efficient.

## 4.7 Conclusion

When looking at the finished ROV-frame, its appearance, and its shape, it is clear to see that it solved the initial challenges it was meant to solve. It has an efficient design, allowing for easy implementation of various equipment. The ROV-frame is also less complex than it would be otherwise due to the implementation of the DFA concept. Working together with the UiS Subsea motor control group, an efficient placement of the thrusters was achieved, which allowed for full control authority of the ROV. Due to the many restrictions regarding the Covid-19 pandemic, the shipping of several important parts needed for the electronic control of the ROV did not make it in time.

This resulted in the ROV not being tested within the time frame for this thesis. However, the ROV-frame was manufactured according to the initial Gantt project plans, which is also an indication of the success of the project.

*Figure 4.23 – Apex Multicam CNC router, cutting side plates*

If the ROV were to be further developed and taken into mass production, the components manufactured by a specialist manufacturer would use little to no extra capacity to produce more units. As an example, the side plates of the ROV made of PE plastic, are delivered in plates of 3 x 1,5 m. Each side plate fits within a dimension of 0,3 x 0,4 m, this means that for the same amount of work programming the machine, as seen in Figure 4.23, for material type and assignment, it can produce 37 units without human interaction. This frees up manpower to perform other tasks than manually machining each side plate in a milling machine and will significantly lower the cost of production while at the same time produce side plates for 18 ROV's, with relatively low production time.

Calculating values for metrics such as design efficiency, total assembly time, quality of design, complexity factor and total assembly cost gives us measurable metrics to indicate the project's success (Ezpeleta, et al., 2019).

$$Design\ efficiency\ (D_E) = 100 * \frac{\sum A}{\sum A + \sum B}$$

A = essential part, B = non-essential part

By using part list from Table 4.1, the essential parts are counted and compared with the non-essential parts. All parts are considered essential except the corner covers, this gives a design efficiency of 94%. This result is very satisfactory for a prototype design and was achieved by countless iterations during the design process. By developing the ROV further, a design efficiency closing in on 100% could be possible.

$$Total\ assembly\ time\ (TAT) = \sum T_H + \sum T_I$$

$T_H$ = handling time, $T_I$ = insertion time

The manufacturing process of the ROV included 16 hours for producing parts, and 24 hours for assembly. This equates to $T_H$ = 16, $T_I$ = 24, for a total assembly time of 40 hours.

$$Quality\ of\ design\ (Assemblability\ Ratio, A_R) = 100 * \frac{2{,}35 * \sum A}{TAT}$$

2,35 = constant

The quality of design is a measure of the DFA process that took place in the very beginning of this thesis. It takes into consideration the essential part, multiplied with an equation constant, and dividing by the total assembly time (TAT). The design quality was measured to be 0,54%. This figure is affected by the total amount of parts as well as the total assembly time. Considering this is a prototype, and the measured time was the first time the ROV was built, there is a lot of improvement to gain in perfecting the processes.

$$Part\ assembly\ cost, C_C = Hourly\ rate * (T_H + T_I)$$

$$Total\ assembly\ cost, C_T = \sum C_C$$

The hourly rate was taken from NITO – Norges Ingeniør- og Teknologorganisasjon, and calculated to be 325 NOK, which is quite high considering this work could be outsourced for quite a bit cheaper.
The total assembly cost for the ROV prototype amounted to a total cost of 2 x 13 013 NOK, which amounts to 26 026 NOK.
These values indicate that although the design has a very good efficiency, the overall manufacturing and assembly process still has areas of improvement. This is something that could be improved during further development of the ROV prototype. The values found for total assembly time would have decreased per extra unit produced, this would have resulted in a lower assemblability ratio which would have contributed to a lower assembly cost.

# 5 Thruster analysis

## 5.1 Content in this chapter

- Introduction (to the ROV movement)
- Required motion
  - Choice of thruster
- Number and placement of thruster
- Forces and thrust analysis
  - Angle of the horizontal thrusters
  - Vector forces and control authority
  - RPM control using PWM signal
  - Propeller theory
- Thruster-Thruster interaction

## 5.2 Introduction

The ROV would need to have six degrees of freedom, meaning full control to translate in the X-, Y- and Z-axis. It should also have the ability to rotate in pitch-, yaw- and roll-axes. Six degrees of freedom refers to the full motion of movements the ROV would be capable to perform in the real world, as shown in Figure 5.1. Choosing the correct thruster motor, thruster housing and propeller design, while also considering a suitable number of thrusters in an appropriate configuration to allow for six degrees of freedom was an important factor in the overall design of the ROV. Considerations such as the torque imposed by an object captured by the manipulator arm would guide the placement of the vertical positioned thrusters in order to cancel out any forces. These considerations were made based on the mission objectives presented in the MATE competition. The maximum weight applied on the extended manipulator arm during the competition will be 0,5 kg or less at its gripping point, this allows for calculations to be made taking into consideration the total length and weight of the manipulator arm.

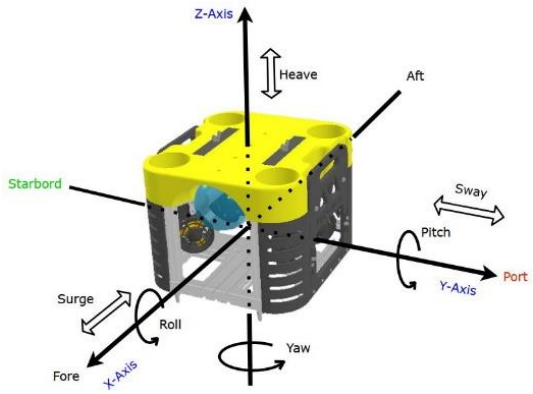


*Figure 5.1 – Graphical representation of the ROV and its six degrees of freedom*

## 5.3 Required motion

The ROV will be capable of carrying a payload, and so the required thrust would have to reflect this weight as well as compensate for the tasks that the manipulator arm must be able to perform during the MATE competition. The manipulator arm extends approximately 50 cm out from the frame and will apply a larger torque the further the arm extends from the centre of mass of the ROV.

The project could not afford having thrusters that would provide too little thrust force, potentially inhibiting the performance of the ROV in use. Cost was also an important factor in choosing suitable motors for the thrusters and would affect the overall project in respect to placement, power budget and manoeuvrability. UiS Subsea went on a field excursion to Oceaneering at Tau just outside Stavanger, visiting their Autonomous Underwater Vehicle (AUV) Freedom, UiS Subsea was recommended to reach out to Thrustme AS for thruster applications. Thrustme AS is a local company specializing in water activities and wanted to contribute to the project with suitable thrusters and electronic speed controllers (ESC) for the ROV. After reviewing the thruster and ESC specifications together with the team responsible for motor control, it was decided to go ahead with testing and analysis of the thrusters.

### 5.3.1 Choice of thruster

Torque and speed control were important due to the need of quick and precise repositioning of the ROV, this required a thruster motor with good response and high torque at low revolutions per minute (RPM). This characteristic can be seen in Figure 5.2 in the intermittent torque zone (Yedamale, 2009).

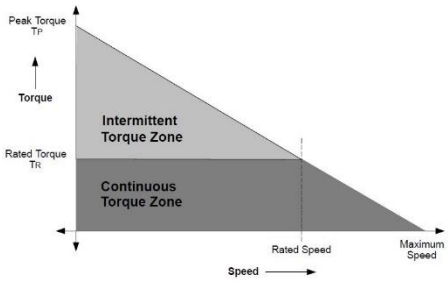


*Figure 5.2 – Torque to speed characteristics*

Thrustme AS provided a thruster configuration consisting of a brushless direct current (BLDC) motor mounted within a housing and fitted with a propeller. The thruster configuration would be able to run in a direct current (DC) voltage range of 12 - 25,2 volts. This performance falls in a range needed for the ROV as the motor is capable of being adjusted to low voltages while still being able to provide high torque. The total weight of the thruster configuration was measured to be in the range of 0,8 – 0,82 kg with a 1,3-meter cable, which was on the high end considering the weight restrictions set in place by the MATE competition.

Considering the operating depth of the ROV of 100 meters at a hydrostatic pressure of 1,1 MPa as shown in sub-chapter 7.2.1, the thrusters will be more than capable with their depth rating of approximately 30,3 MPa. The depth rating of the thrusters gives a safety factor of approximately $\frac{30,3}{1,1} \approx 27,5$ against water intrusion.

## 5.4 Number and placement of thrusters

Several thruster configurations were considered, ranging from two to three vertical thrusters and the same amount for the horizontal ones. An even number of vertical thrusters will give good overall control needed to position the ROV correctly and efficiently in the environment, with or without additional payload. The horizontal thrusters would have to take into consideration translative motion in the X- and Y-axes as well as yaw and roll. Bearing in mind the potential payload weight, a total of eight thrusters were chosen to provide sufficient amount of control authority in X-, Y- and Z-axes as well as pitch, yaw and roll. It was desirable to place the thrusters as far out from the centre of mass as possible in order to reduce the inertia around the axes of rotation and increase stabilization control. Due to the fact that most tasks in the MATE competition are to be performed with the use of a manipulator arm which applies torque in the pitch axis, the vertical thrusters were prioritized furthest out to more easily neutralize the torque while at the same time having enough force to heave the ROV. This at the expense of the horizontal thrusters which will have a greater inertia as they must be placed slightly closer to the centre of mass to avoid thruster-thruster interaction or blockage. To have a robust design, the thrusters were placed inside the frame to withstand any collisions that may occur during the competition. Thruster placement can be seen in Figure 5.3 with the dimensions shown in Table 5.1. The position of the thrusters was placed in such a way that they would act furthest away from the centre of mass all while having the least possible thruster-thruster interaction.

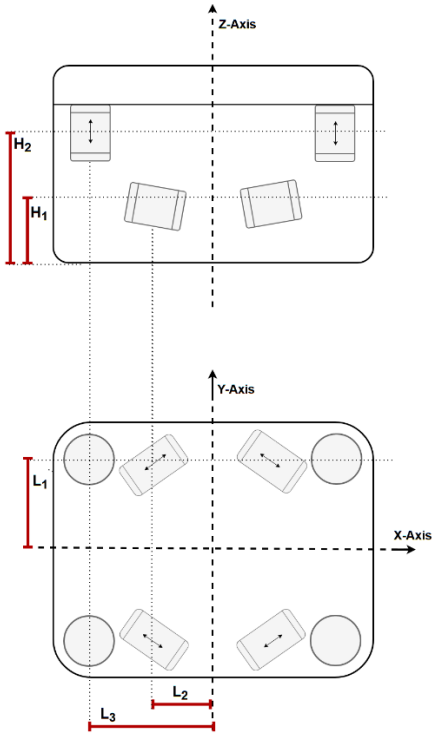


*Figure 5.3 – Thruster placement*

*Table 5.1 – Thruster Distances, in Figure 5.3*

| **Thruster Placement** | |
|---|---|
| Designation | Distance (mm) |
| **$L_1$** | 170 |
| **$L_2$** | 137 |
| **$L_3$** | 180 |
| **$H_1$** | 115 ± 30 |
| **$H_2$** | 165 |

## 5.5 Forces and thrust analysis

The performance testing of the thruster was executed locally at the University of Stavanger, using a water container and a leverage system for measuring the provided thrust force of the thruster. The leverage system consisted of a 2:1 relationship ensuring full water coverage of the thruster, while measuring the provided thrust with a Kern CH 50 K 50 digital scale. The total budget for power control of the thrusters were set to 12-volt DC with a maximum of 1200 watt where each thruster was limited by a 16-ampere fuse. Following the power equation, the maximum power drain for each motor was calculated:

$$P = V * I$$

Filling in values:

$$P = 12V * 16A$$

$$= \underline{192\ W}$$

The thruster was tested at 12 volts DC up to a total power drain of 192 watts and 16-amperes. Thrust forces at increments of 20 watts were recorded and plotted in Figure 5.4, the values indicate a drop in efficiency in counter-clockwise (CCW) rotation compared to clockwise (CW) rotation. This is especially prominent from approximately 70 watts onward. A maximum thrust force of 58 N was recorded during CW rotation, and 49 N at CCW rotation yielding a total difference of 15,5%. Seeing that the thrusters are giving different values when powered in CW and CCW rotation respectively, the overall thrust force of each thruster on the ROV is electronically regulated to a maximum thrust of 49 N. This is done to eliminate torque forces and any disturbances that would occur during movement with unequal thrust force. The magnitude of thrust forces in surge and sway motion is decomposed and shown in Table 5.2.

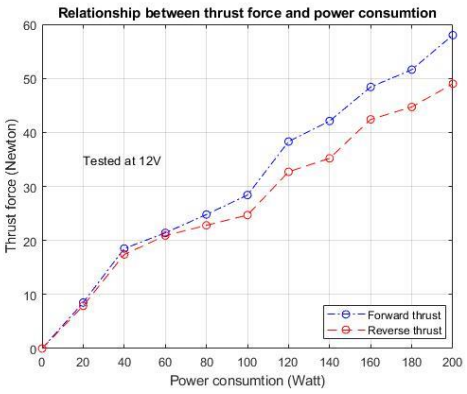


*Figure 5.4 – Thrust tested against power consumption*

### 5.5.1 Angle of the horizontal thrusters

To ensure appropriate distribution of forward motion and sideways translation, it was crucial that the angle of the horizontal thrusters was optimized for the tasks at the MATE competition. During the field excursion to Oceaneering at Tau, inspiration on horizontal thruster angles were taken from the AUV Freedom. Seeing Freedom is used for long underwater surveys of oil- and gas lines, it uses angled thrusters in an orientation of 30° relative to its central axis, as shown in Figure 5.5. This orientation ensures efficient translation along the seabed while still offering good rotation when needed. The tasks in the MATE competition requires good manoeuvrability from the competing ROV's, while still being able to move quickly from task to task. An angle of 45° on the horizontal thrusters will give equal forces in both the X- and Y-axis resulting in an ROV with equal capabilities in rotational and translational movement, forces decomposed in angles from 25° to 45° can be seen in Table 5.2. Translational movement is preferred, and so an appropriate angle below 45° will have to be determined to achieve this. Any angle above 45° will result in the ROV favouring rotational and sway movement.

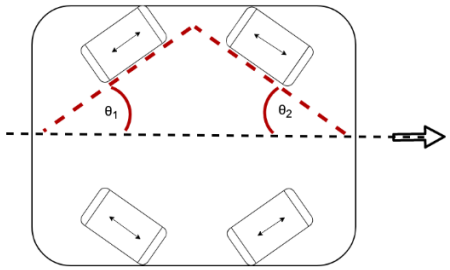


*Figure 5.5 – Thruster angle relative to central axis*

*Table 5.2 – Decomposed thrust forces in surge and sway motion*

| Thrust force<br>F | Angle<br>θ (°) | Force resulting in surge<br>$\boldsymbol{F * \cos\theta}$ (N) | Force resulting in sway<br>$\boldsymbol{F * \sin\theta}$ (N) |
|---|---|---|---|
| 49 N | 25 | 44,4 | 20,7 |
| " | 30 | 42,4 | 24,5 |
| " | 35 | 40,1 | 28,1 |
| " | 40 | 37,5 | 31,5 |
| " | 45 | 34,6 | 34,6 |

Looking at the calculated values in Table 5.2, the forces at an angle of 35° was chosen giving a desired relation between surge and sway. Surge would in this case be favoured by 81,8% of the total force of 49 N, while sway would generate 57,3% of the total force of 49 N. Compared, surge would have a 30% advantage over the force from sway resulting in more thrust being generated in the X-axis which causes fore and aft movement. Combined, the forces in X- and Y-axis will give, based on the Pythagorean theorem:

$$c^2 = a^2 + b^2$$

Solving for c:

$$c = \sqrt{a^2 + b^2}$$

$$c = \sqrt{40{,}1^2 + 28{,}1^2} = \underline{\underline{49\ N}}$$

A graphical representation of the forces in surge and sway can be seen in Figure 5.6, in red and blue colours, respectively. The thrust force, decomposed into forces of surge and sway, translates into motion, and is depicted by the purple arrow.

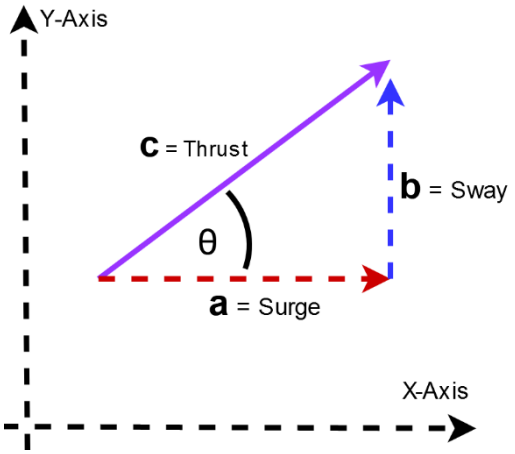


*Figure 5.6 – Graphical representation showing decomposed forces*

### 5.5.2 Vector forces and control authority

Movement of the ROV is a result of a combination of thruster inputs. Thrust force values previously calculated, gives initial values for calculating the combination of thrusters needed for any required motion. Placement of the horizontal and vertical thrusters can be seen in Figure 5.7. Considering the right-hand rule, a combination of thruster inputs represented by a positive or negative sign, will be activated to yield the desired motion. This can be seen in Table 5.3 for the vertical movement, and in Table 5.4 for horizontal movement. Each horizontal thruster will give an input thrust force of 40,1 N in the X-axis, and 28,1 N in the Y-axis. Furthermore, each vertical thruster will give a thrust force with the magnitude of 49 N in the Z-axis.

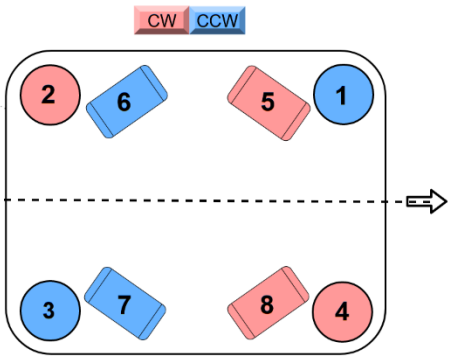


*Figure 5.7 – Graphical representation of numerical thruster placement*

*Table 5.3 – Vertical thrust forces, vector direction in Z-Axis for desired movement*

| Movement | Heave (+) | Heave (-) | Pitch (+) Around (Y) | Pitch (-) Around (Y) | Roll CCW Around (X) | Roll CW Around (X) |
|---|---|---|---|---|---|---|
| **Thruster** | z | z | \|z\| | \|z\| | \|z\| | \|z\| |
| **1** | + | - | - | + | + | - |
| **2** | + | - | + | - | + | - |
| **3** | + | - | + | - | - | + |
| **4** | + | - | - | + | - | + |
| **SUM** | 196 N | -196 N | 196 N | 196 N | 196 N | 196 N |

*Table 5.4 – Horizontal thrust forces, vector direction in XY-Plane for desired movement*

| Movement | Surge (+) | | Surge (-) | | Sway (+) | | Sway (-) | | Yaw (+) | | Yaw (-) | |
|---|---|---|---|---|---|---|---|---|---|---|---|---|
| **Thruster** | X | Y | X | Y | X | Y | X | Y | \|X\| | \|Y\| | \|X\| | \|Y\| |
| **5** | + | - | - | + | - | + | + | - | - | + | + | - |
| **6** | + | + | - | - | + | + | - | - | - | - | + | + |
| **7** | + | - | - | + | - | + | + | - | + | - | - | + |
| **8** | + | + | - | - | + | + | - | - | + | + | - | - |
| **SUM** | 160 N | 0 | -160 N | 0 | 0 | 112 N | 0 | -112 N | 160 N | 112 N | 160 N | 112 N |

Using Autodesk's simulation tool for Computational Fluid Dynamics (CFD), which is a tool for analysing an objects movement or properties in a certain environment using complex numerical methods. In this case a solid object in motion through fluid, where the ROV was simulated to run in seawater with a density of 1025 kg/m$^3$, with the thrust force values shown in Table 5.5. By using the results from the

CFD analysis, design and structural factors can be further developed if the simulation shows that the hydrodynamic properties of the ROV appear to have significant limitations. Thus, one can detect this at an early stage in the design phase, which reduces the need for prototyping and experimental testing which is both time consuming and costly.

*Table 5.5 – Numerical values from CFD simulation*

| | **Surge** | **Sway** | **Heave** |
|---|---|---|---|
| **Thrust (N)** | 160 | 112 | 196 |
| **Drag** | " | " | " |
| **Area perpendicular to direction of travel** $(m^2)$ | 0,1563 | 0,1664 | 0,2581 |
| **Terminal velocity** $(^{m}/_{s})$ | 1,51 | 1,18 | 1,16 |

The values from Table 5.5, are used to determine the drag forces that are applied to the ROV due to it moving at a different speed than its surroundings. These calculations are based on the assumption that there are no currents in the water, that the Reynolds number (Re) ≥ $10^4$ and that it does not have an umbilical cord that goes up to the control station. Final specifications regarding size and weight of the umbilical cord are still to be determined, this uncertainty is something that will affect the drag results achieved in the simulation as well as rough sea conditions which would slow the ROV down. In the simulation the ROV was tested from a standstill until the drag force was equal to the thrust force, as this will be a theoretical terminal velocity.

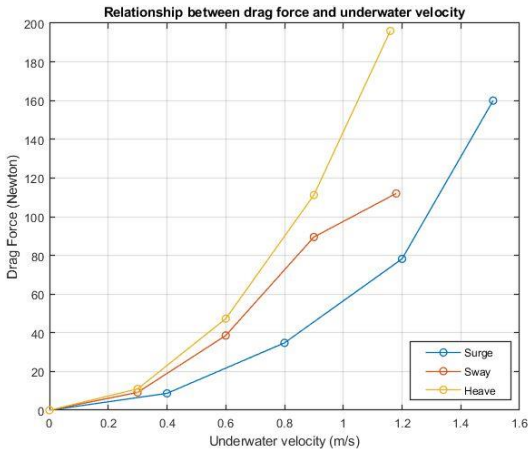


*Figure 5.8 – Numerical values between drag force and underwater velocity*

The values of this simulation are shown in Figure 5.8. Theoretically, this indicates that the ROV will have the

opportunity to surge in a speed of 1,51 m/s, sway in 1,18 m/s and heave in 1,16 m/s with the hydrodynamic analysis results shown in Figure 5.9.

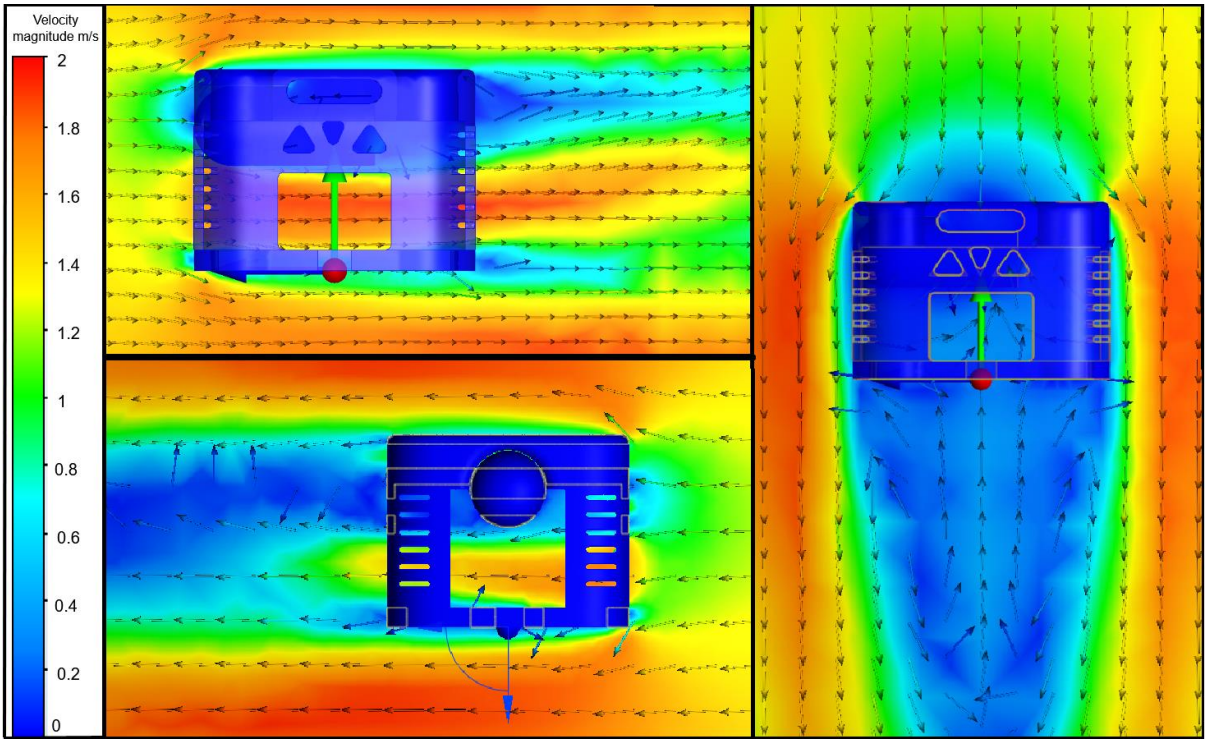


*Figure 5.9 – CFD analysis during Surge (top left), Sway (lower left), and Heave (right)*

By using the drag force equation:

$$F_D = \frac{1}{2}\rho C_D A U^2$$

And solving for the coefficient of drag, $C_D$:

$$C_D = \frac{2F_D}{\rho A U^2}$$

The numerical values of $F_D$ when equal to $F_T$ derived through CFD analysis can be used to determine the coefficient of drag of the ROV. Filling in numerical values determines $C_D$ to be:

$$C_{D,X} = \frac{2*160}{1025*0.1563*1{,}51^2} = \underline{0{,}876}$$

$$C_{D,Y} = \frac{2*112}{1025*0{,}1664*1{,}18^2} = \underline{0{,}943}$$

$$C_{D,Z} = \frac{2*196}{1025*0{,}2581*1{,}16^2} = \underline{1{,}1}$$

The coefficient of drag calculated above is deemed to be theoretical under ideal circumstances. The drag coefficient should ideally be confirmed through experimental testing.

It is important to establish the amount of torque that is applied by the manipulator arm to the ROV. And then what amount of force the ROV needs to counteract the torque with, in order to manipulate objects in the competition and bring them to the surface. This is done by calculating the distances and forces that are applied around the pivot point, y-axis, which in this case is at the center of the ROV during pitch. The maximum weight the manipulator arm is going to see during the competition is 5 N, and the extension length outside the ROV-frame is a maximum of 0,5 m. The length of the ROV is 0,545 m, so a force with maximum extension on the manipulator arm would provide torque a total distance of $\frac{0.545\ m}{2} + 0.5\ m = 0{,}7725\ m$ from the pivot point and around the Y-Axis. And from Table 5.1 – Thruster distances, the distance $L_3$ = 0,18 m is the distance that the vertical thrusters act from the Y-axis which they will apply torque around given that thrusters 2 and 3, operate in the opposite direction than thrusters 1 and 4 seen in Figure 5.7. The vertical thrusters combined gives a maximum force of 196 N in the Z-Axis. The maximum possible force applied by the manipulator arm while still being able to hold the ROV in equilibrium can be calculated by:

$$\sum \tau_y = 0$$

$$F_{manipulator} * 0.7725\ m - 196\ N * 0.18\ m = 0$$

$$F_{manipulator} = \frac{196\ N * 0.18\ m}{0.7725\ m} \approx \underline{\underline{45.7\ N}}$$

The forces needed to hold the ROV in equilibrium with the manipulator arm carrying the 5 N as stated in the MATE Competition will be:

$$F_{thrusters} = \frac{5\ N * 0.17725\ m}{0.18\ m} \approx \underline{\underline{21.5\ N}}$$

This means that the remaining forces $196\ N - 21.5\ N = \underline{\underline{174.5\ N}}$ can be used explicitly to heave the ROV while performing the designated tasks.

### 5.5.3 RPM control using PWM signal

During testing and operation of the ROV, the thruster's RPM is controlled by a pulse-width modulated (PWM) signal in the range of 1100-1900 µs provided by an Arduino Uno microcontroller. The microcontroller ran a specified code to regulate the thruster motor, this regulation provided necessary control authority by limiting the RPM a thus the thrust force. Power for the thruster motor was provided by a 12-volt DC power supply. The PWM signal as seen in Figure 5.10 is a square wave signal similar to a sinusoidal wave generated by AC-voltage, only without the negative period of the signal. The signal is controlled in percentage of the full period by switching the signal ON and OFF, this in turn effectively regulates the thruster RPM. During use, the ROV will implement one ESC for each of the thrusters. The ESC is an electronic device which allows the onboard control system to adjust the thrust force of each thruster separately precisely and efficiently by regulating the RPM. Previous ROV's designed and built by UiS Subsea have implemented the ESC's inside the electronics container, contributing to thermal heating of the container and its components. The 2021 UiS Subsea team will mount the ESC's outside of the electronics container, ensuring efficient cooling by the surrounding water. Mounting of the ESC's outside of the electronics container imposes its own challenges in respect to watertightness. At a depth of 100 meters the hydrostatic pressure is approximately 1,1 MPa as shown in sub-chapter 6.2.1. The supplied ESC's have a depth rating of more than 2,6 MPa, which is well beyond the requirements for this project and gives the ESC's a safety factor of almost $\frac{2,6}{1,1} \approx \underline{2,4}$ against water intrusion.

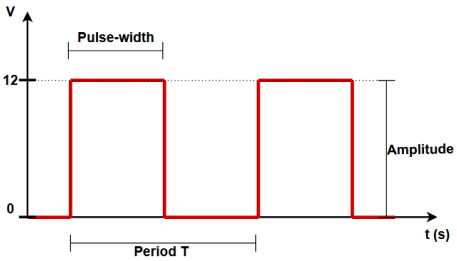


*Figure 5.10 – PWM signal*

### 5.5.4 Propeller theory

The propeller fitted to the thruster assembly provided by Thrustme AS had a fixed geometry, three blade design. A three-blade propeller design is a compromise between efficiency and vibrations. Most propellers are made with three blades, the compromise between efficiency is considered to be less significant than any differences in vibration. The geometry of the propeller blade takes into consideration the pitch angle of the propeller blade compared to its axial flow direction and is defined based on the advancing distance per revolution with no slip, similar to a wood screw. The pitch works in direct relation with motor RPM, too low pitch and the motor will run at a higher RPM potentially putting unnecessary stress on the motor and other rotating parts. Higher as well as lower RPM will result in a change of the thruster's efficiency. Two types of pitch are commonly used in propeller design, they are constant pitch also known as "true" or "flat" pitch, and progressive pitch. Progressive pitch propellers have a shallow angle on the leading edge of the propeller, increasing towards the trailing edge. Progressive pitch propellers are mostly used when high translational and rotational

speed is needed. There also exists a mechanical adjustable pitch design used to allow for optimum thrust for a marine vessel according to any change in cruise conditions such as load and speed. (Ulgen, 2013). The propeller fitted to the thruster assembly from Thrustme AS has a decreasing pitch angle, starting steep at the base diameter of the propeller and decreasing towards the tip of the propeller. The propeller design takes into consideration the tangential velocity in the equation for angular velocity:

$$v = r\omega$$

Seeing the propeller velocity is higher at the tip of the propeller blade than it is at the base, the pitch will have to decrease to maintain a near constant angle of attack. Angle of attack is the angle between the chord, as can be seen as a dotted line through the wing in Figure 5.11, and the relative wind that the wing sees. The angle of attack creates a pressure difference above and below the wing and it is this pressure difference that creates lift by implementing Bernoulli's equation and Newton's third law that states each action has an equal and opposite reaction. The angle of attack acting on a wing can be seen in Figure 5.12. The shape of the propeller is similar to the shape of an aircraft wing, and therefore it can be helpful to compare how a propeller blade works to how an airplane wing works.

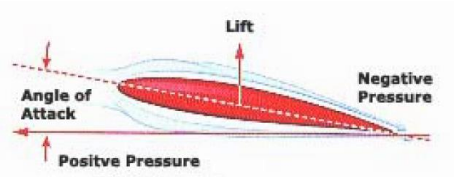


*Figure 5.11 – Pressure difference due to angle of attack*

*(a)* *(b)*

*Figure 5.12 – Effect of angle of attack on a wing. (a) No angle of attack, and (b) Pressure difference created by angle of attack (Marine, 2004).*

Similar to an aircraft wing, the propeller used in the thruster assembly has an angle of attack that creates lift, or in this case thrust. Zero angle of attack would not create any positive or negative pressure, resulting in no thrust created. Looking at Figure 5.13, rotational forces can be divided into a thrust component in the direction of travel, a torque component opposite of the propeller rotation, and lift approximately normal to the surface of the propeller blade. Slip is the difference between actual and theoretical advancing distance per revolution, and it results from the propeller angle of attack. Therefore, to create lift, or in this case thrust there must be some angle of attack or slip (Marine, 2004).

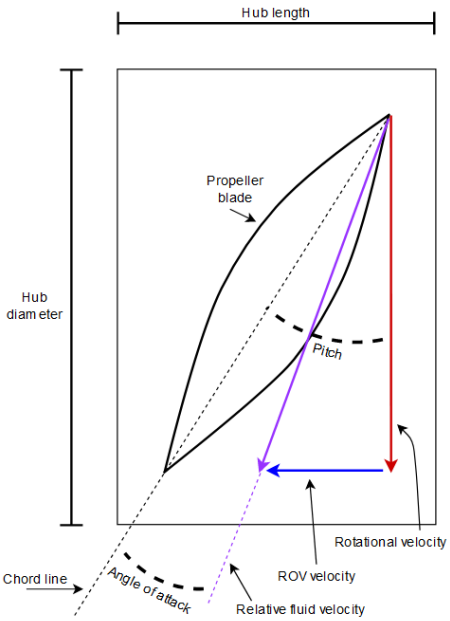

*Figure 5.13 – Rotational forces decomposed*

During operation, the thruster assembly will generate a thrust of 49 N. This thrust is below the maximum rated 157 N stated in the datasheet, however there is still a need to know the maximum deflection of the propeller blades at operating thrust. By analysing the stresses induced on the propellers during operation, a decision can be made on alternatively producing the propellers out of another material to reduce weight. A stress analysis using Autodesk Inventor were performed on the propeller blades. The thrust force provided by the propeller was assumed to be equally split on each of the three propeller blades, resulting in a force of 16,3 N acting on each blade. The stress analysis calculated a maximum displacement of $4{,}626 * 10^{-1}$ mm at the tip of the propeller blades as can be seen in Figure 5.14, which were considered acceptable. Calculations also revealed a maximum von Mises stress value of 7,802 MPa. The propeller blades are constructed of glass filled polyurethane with a rated tensile yield strength of between 52,4 – 79,3 MPa, this means the propellers will be more than strong enough with a safety factor of nearly $\frac{52{,}4}{7{,}802} \approx \underline{6{,}71}$ against yield or fracture according to the lowest tensile strength value. The values for von Mises stress can be seen in Figure 5.15 where it becomes clear that the highest amount of stress occurs at the base of the

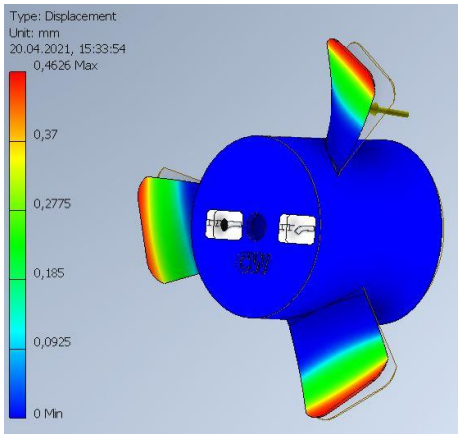

*Figure 5.14 – Maximum deflection of propeller blades*

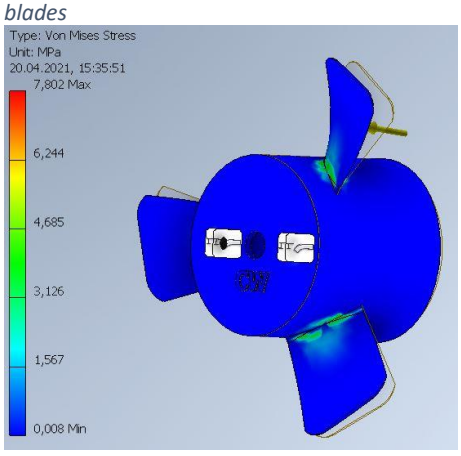

*Figure 5.15 – Maximum von Mises stress at a thrust force of 49 N*

propeller hub. This is where the propeller attaches to the rotating hub and where the force of rotation is converted to thrust (Marine, 2004).

## 5.6 Thruster-Thruster interaction

Due to the horizontal thruster configuration, thruster to thruster interactions could limit the incoming flow seen by the downwind thruster. During operation, the propeller blades will create low- and high-pressure zones that will migrate from the centre of the propeller, towards the tip of the propeller blades where they will meet and form tip vortices that cause turbulence (Koh K. K., 2015). In an un-ducted thruster design the turbulence will cause increased drag, noise and heat and will result in a less efficient thruster. By using a thruster fitted with a duct enclosure that encases the propeller and directs incoming flow as well as outgoing thrust in axial directions through the centre of the thruster, the tip vortices will be reduced, and efficiency of the thruster will be higher. The duct fitted to the thruster used on this ROV has a duct shaped similar to the nozzle designed by Maritime Research Institute Netherlands, MARIN 37 as can be seen in Figure 5.16. It is considered to be an accelerating duct, meaning that the inflow velocity and the efficiency of the propeller is increased. (Carlton, 2012). The horizontal thrusters are angled 35° degrees outward from a central X-axis running through the ROV, as seen in Figure 5.17 together with thruster activation for desired movement.


*Figure 5.16 – MARIN 37 nozzle design*

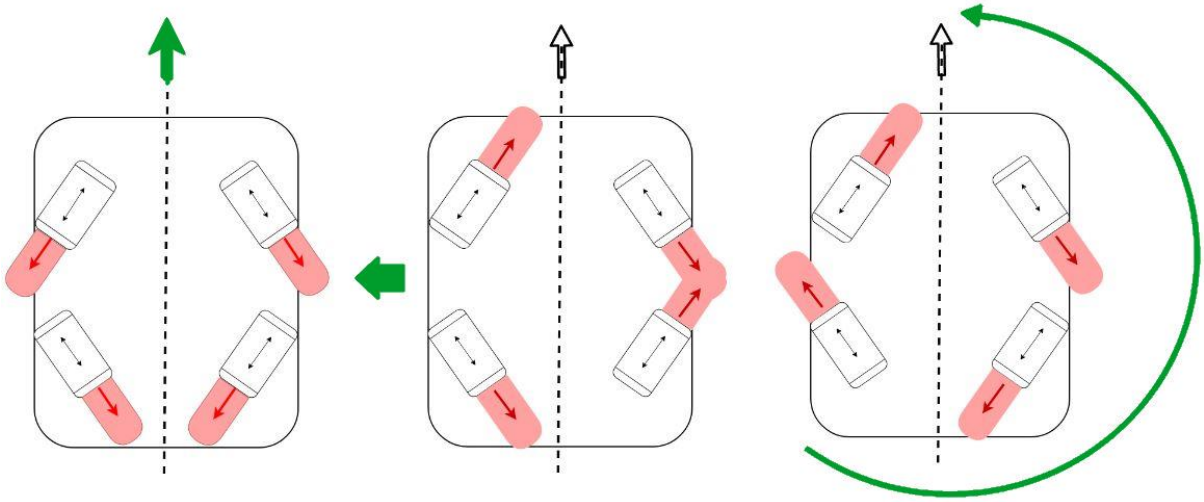

*(a)* *(b)* *(c)*

*Figure 5.17 – Horizontal movement of the ROV represented by green colour. Overhead view of: (a) Surge, (b) Sway, (c) Yaw*

There is a combined angle between the thrusters of 110°, this means there is a slight interference between the thrusters, compared to the thrusters being fitted perpendicular to each other with a relative angle of 90° between each other. Limited available space due to the ROV being specialised towards competing in the MATE competition will result in some thruster-to-thruster interaction occurring.

The interaction itself is deemed to be of little relevance seeing the low velocity the ROV will be operated at. Thruster repositioning based on CFD analysis would have to be performed to analyse its effects and to potentially achieve a more accurate placement.

## 5.7 Conclusions

Considering the tasks the ROV is set to perform, the thruster configurations that are based on theoretical calculations is deemed satisfactory. Based on calculations the ROV seems to have a very good range of motion, with six degrees of freedom. Due to time constraints, the design had to implement a less-than-ideal solution for the horizontal thruster placement. The thrusters will have some interaction during operation, although not deemed to be critical, it still is an area to be improved upon during future development. The vertical thrusters have a very efficient placement in regard to eliminating torque imposed on the ROV by the manipulator arm.

# 6 Additional contributions to the UiS Subsea team

## 6.1 Content in this chapter

- Mechanical calculations and dimensioning of aluminium electronics container
- Design consultations and optimalisations regarding the Micro ROV
- Machining of the cooling fins used in the electronic cupola

## 6.2 Introduction

During the project, several groups in UiS Subsea reached out in need of assistance and guidance. Seeing there where some form of mechanical aspect in most groups such as dimensioning the proper thickness of the electronic container, designing innovative and smart solutions for 3D-printing the micro-ROV, or machining parts in the workshop among others, it was natural to provide some assistance. Support was given in addition to the work already allocated and was performed in parallel with existing tasks. There were several contributions to the groups in UiS Subsea, where some of them are listed below. Many of the contributions directly affected the completion of the UiS Subsea project in a timely and professional manner, ensuring efficient and steady progress of the project.

### 6.2.1 Mechanical calculations regarding the electronic container

One of the contributions was to help the electrical engineers with the design of the electronic container, it was desirable with the largest possible volume at the same time as there should be room for a connector plate in the rear of the container and a clear dome in front without it protruding from the frame design. The mechanical team had an open dialogue with the group that was to produce the container. Together the groups arrived at an optimal length of 300 mm, not considering the rear connector plate and front dome, which would make it easy to distribute the available space to different electrical groups.

It was desirable to have an outside diameter of 160 mm to be able to contain all the electronics, while still being able to fit within the frame design. Calculating the hydrostatic pressure at 100 meters in seawater was done using the equation:

$$P = P_0 + \rho g h$$

Table 6.1 is showing the symbol descriptions and values for necessary calculations:

*Table 6.1 – Symbol description*

| Symbol | Description | Values |
|---|---|---|
| **P** | Operating pressure | ? |
| **$P_0$** | Atmospheric pressure | 101325 Pa |
| **ρ** | Density (seawater) | 1025 $kg/m^3$ |
| $\boldsymbol{g}$ | Gravitational acceleration | 9,81 $m/s^2$ |
| $\boldsymbol{h}$ | Depth | 100 m |
| **t** | Material thickness | ? |
| **D** | External diameter | 160 mm |
| **ν (nu)** | Poisson ratio | 0,33 (6061-T6 Alu.) |
| **E** | Young's modulus | 69 GPa (6061-T6 Alu.) |

Filling in values:

$$P = 101325\ Pa + 1025\frac{kg}{m^3} * 9{,}81\frac{m}{s^2} * 100\ m$$

$$= 1106850\ Pa \approx \underline{\underline{1{,}1\ MPa}}$$

By this result the calculations show the hydrostatic pressure at a depth of 100 meters in seawater is approximately 1,1 MPa, which is the minimum pressure the aluminium container will need to withstand to resist implosion.

The formula for calculating critical external pressure of a pipe is then used to solve for the minimum thickness needed to be able to withstand a hydrostatic pressure of 1,1 MPa:

$$P_{crit} = \frac{2E}{(1-\nu^2)} * (\frac{t}{D})^3$$

Solving for t:

$$t = \sqrt[3]{\frac{P_{crit} * (1-\nu^2)}{2E}} * D$$

Filling in values in the equation:

$$t = \sqrt[3]{\frac{1{,}1\ MPa * (1 - 0{,}33^2)}{2 * 69\ GPa}} * 0{,}16\ m$$

$$= 0{,}00308\ m = \underline{3{,}08\ mm}$$

By these calculations, the results are clear that the minimum thickness needs to be 3,08 mm. Due to various circumstances during machining, the external diameter ended up being 162 mm, with a thickness of 3,55 mm. Calculating $P_{crit}$ for these values yielded a result of 1,63 MPa, meaning the aluminium container will be able to reach a depth of approximately 153 meters. This extra depth rating contributes to a pressure safety factor of $\frac{1{,}63}{1{,}1} = \underline{1{,}48}$, which is fair due to the circumstances of which this ROV will operate.

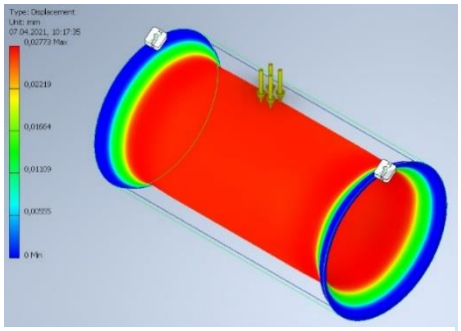

*Figure 6.1 – Stress simulation of aluminium pipe*

As an extra precautionary measure, stress simulations of the aluminium container were performed in Autodesk Inventor, as shown in Figure 6.1, to support the manual calculations. These calculations revealed a maximum displacement of $2{,}73 * 10^{-2}$ mm, which was agreed to be within acceptable values.

Aluminium 6061-T6 was chosen as a material due to weight and strength requirements, good corrosive qualities and material workability. Since it was difficult to get hold of a pipe that would cope with the pressure with the correct dimensions, the pipe had to be machined out of a solid block of aluminium using a lathe. The result was an aluminium container with a thickness of 3,55 mm capable of reaching depths beyond 100 meters.

### 6.2.2 Design consultations and optimalisations regarding the Micro ROV

The group responsible for the micro-ROV reached out for design consultations. They needed optimalisations regarding the design of the micro-ROV in the CAD program Autodesk Inventor. There were provided innovative solutions for combining several 3D-printed parts together with electronics in a compact design resulting in reduced weight and parts needed for assembly. One of these solutions where to combine outside screws with a flange design to provide pressure against the main body of the micro-ROV. This ensured an assembly and disassembly to be fast and efficient, as well as making

the production of the parts a whole lot simpler. All in all, the micro-ROV group were satisfied with the assistance, mentioning that the assistance helped them a great deal in reaching a final product.

### 6.2.3 Machining of the cooling fins used in the electronic container

The group responsible for power distribution reached out for guidance and help with machining several cooling fins for cooling their power system. The cooling fins were cast out of blocks of aluminium and needed to be milled to size and have holes for mounting screws machined. Positioning of the holes, and the amount of material to be removed were closely discussed and agreed upon. All in all, the machining was quite easy, and the result had a great impact in the cooling of the power system. The result was parts that had great fitment within the power system and in the electronics container in general, and that contributed to effectively cool the electronics systems.

# 7 Discussions and conclusions

## 7.1 Discussions

The ROV-frame prototype is overall considered a success. Due to the Covid-19 pandemic, and the restrictions set in place, no physical testing was performed. Theoretical calculations and computational simulations are used to verify its performance, but physical testing is needed to validate its operational function. The ROV adheres to the MATE competition weight and size restrictions set in the initial design phase of maximum 35 kg, and a maximum diameter of 75 cm.

By using DFA, the total part count, complexity, and cost of the ROV was reduced. Although the design is very efficient at 94%, the quality of design (assemblability ratio) is not, coming in at 0,54%. The reason behind this value is due to its long manufacturing and assembly time. By producing more units, the quality of design (assemblability ratio) would have yielded a better value. This is due to production efficiency, meaning similar parts could have been produced simultaneously with little extra manufacturing time. The total assembly cost would have been reduced by increasing the efficacy of the production line.

Due to most of the components on the ROV-frame prototype having a large safety factor, the material cost could have been reduced by refining the material thickness or geometry. This would also reduce the weight of the ROV, which can be beneficial in certain operational aspects. Total count of nuts and bolts could most likely have been reduced by analysing the frame structure in further development.

## 7.2 Conclusions

The goal for this thesis was to develop an aesthetically pleasing ROV design by using the concept of Design for Assembly, while also analysing its thrusters and their placement. The ROV was constructed for the student project UiS Subsea to compete in 2021 MATE competition. The development period ran from 15$^{th}$ of January to 15$^{th}$ of May 2021 and was greatly affected by the worldwide Covid-19 pandemic. What should have been a project limited only by one's imagination, ended up being limited by physical presence and shipping hiccups.

The design phase was initiated over Microsoft Teams meetings, using technology as a benefiting factor. Teams were divided into groups of two, this made communications around the individual project responsibilities more manageable. A large part of this thesis included agreeing on a design that would implement all criteria from MATE, as well as a few set by UiS Subsea. There were several design iterations to narrow in on what has become the final prototype design for the ROV.

The Design for Assembly concept was implemented from the very beginning and was a crucial part of the final ROV design. It made the part count lower than what would have been otherwise, this has been proven several times through the project by the countless iterations most of the crucial components underwent. The concept also proved itself during the assembly of the ROV, as most, if not all parts fitted together first time without modifications.

The thrusters were a topic discussed energetically between the teams. Discussions included reusing previous thruster designs, building our own, and reaching out to the industry for sponsorships. Thrustme AS, a local company based in Stavanger was eager to supply UiS Subsea with a set of thrusters and electronic speed controllers. It was later decided that the thrusters would be a good fit for the ROV based on their power consumption, thrust capabilities and price. Pending the decision of what thrusters to go for, several suggestions on thruster configurations were discussed. UiS Subsea decided to use eight thrusters in an arrangement of four vertical, and four horizontal thrusters. The reasoning behind this decision was manoeuvrability, lifting capability in water, stability control, ease of programming, and expandability. Similar setups had been proven by previous teams at UiS Subsea, new this year was that thruster placement would be inside the frame. By having the thrusters inside the frame, nothing could be damaged during operation if one would crash into the surroundings. The design would also resemble the industry working class ROV's that operate in the oil- and gas industry in and around Stavanger.

The ROV-frame prototype, named Hymir, is considered an overall success. The design is aesthetically pleasing to look at, it holds and can quickly replace equipment as needed for the MATE competition, while theoretically having the desired motion needed. The ROV was designed to contain as few parts as achievable, while its parts are designed to have as high efficiency as possible during the time frame, which made it easy to assemble even though it was time consuming. Hymir has lifted UiS Subsea' capabilities and design to a new stage that will give a vital edge when competing in the MATE competition and will by all accounts contribute to the coming teams in the years to come.

# Appendix

*Figure A.1 – Hymir showcasing its (yellow) buoyancy foam at the top, and the electronic container in the centre of the frame*

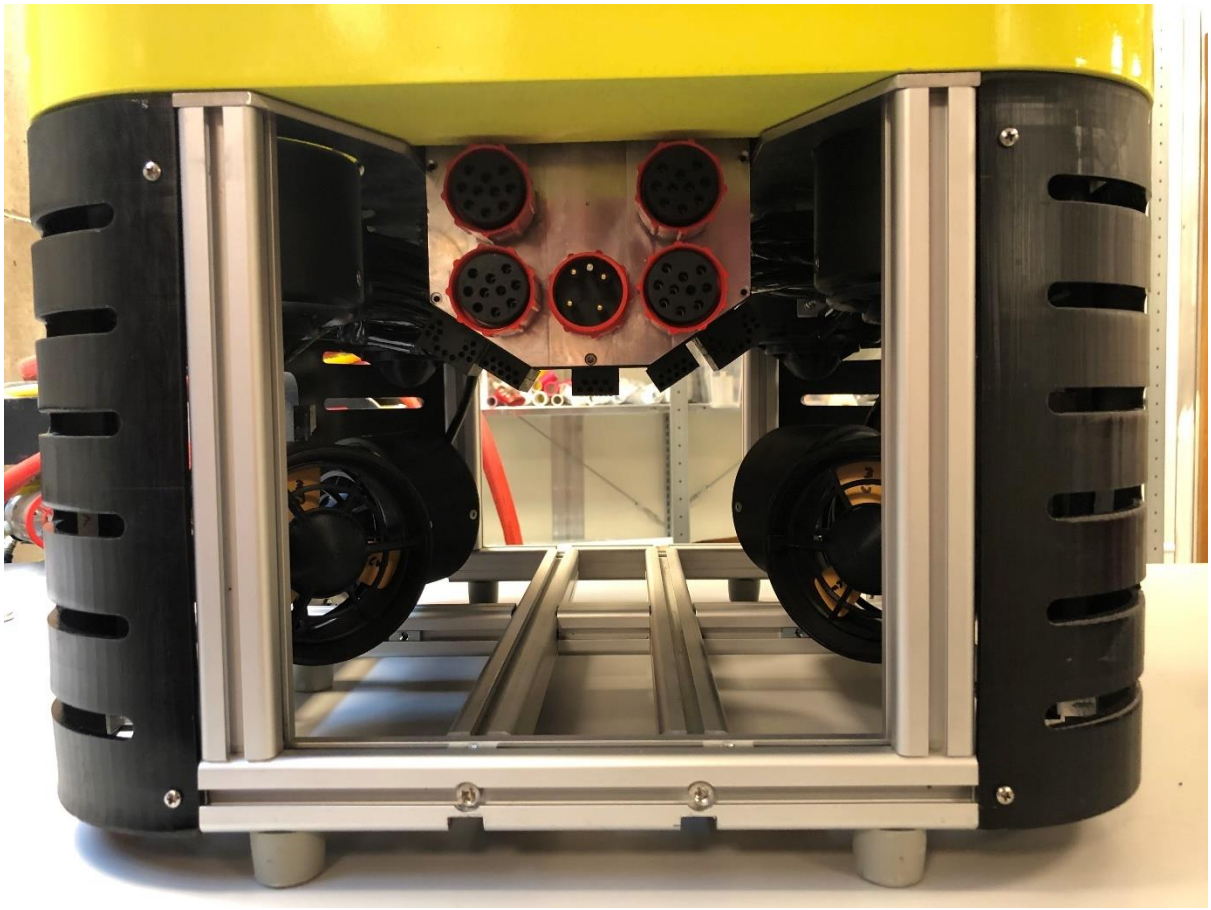

*Figure A.2 – Rear view of Hymir with visible connectors for the electronic equipment*

*Figure A.3 – Rear view of Hymir, showcasing its electronic container and four vertical thrusters*


*Figure A.4 – Hymir fitted with its manipulator arm*


*Figure A.5 – Hymir fishing (as the Norse mythology suggests)*

*Figure A.6 – Hymir presented by Sverd i fjell (Swords in rock)*

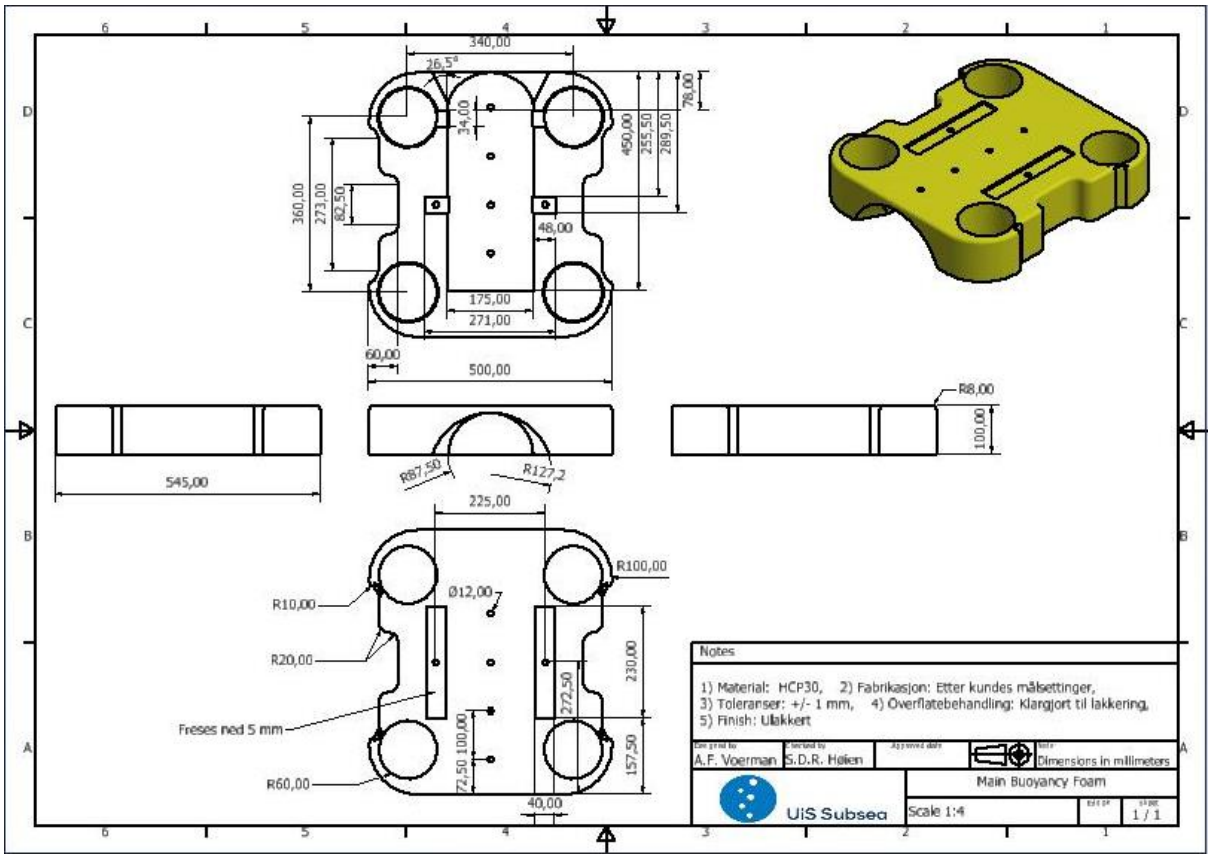


*Figure A.7 – Technical drawing of buoyancy element*

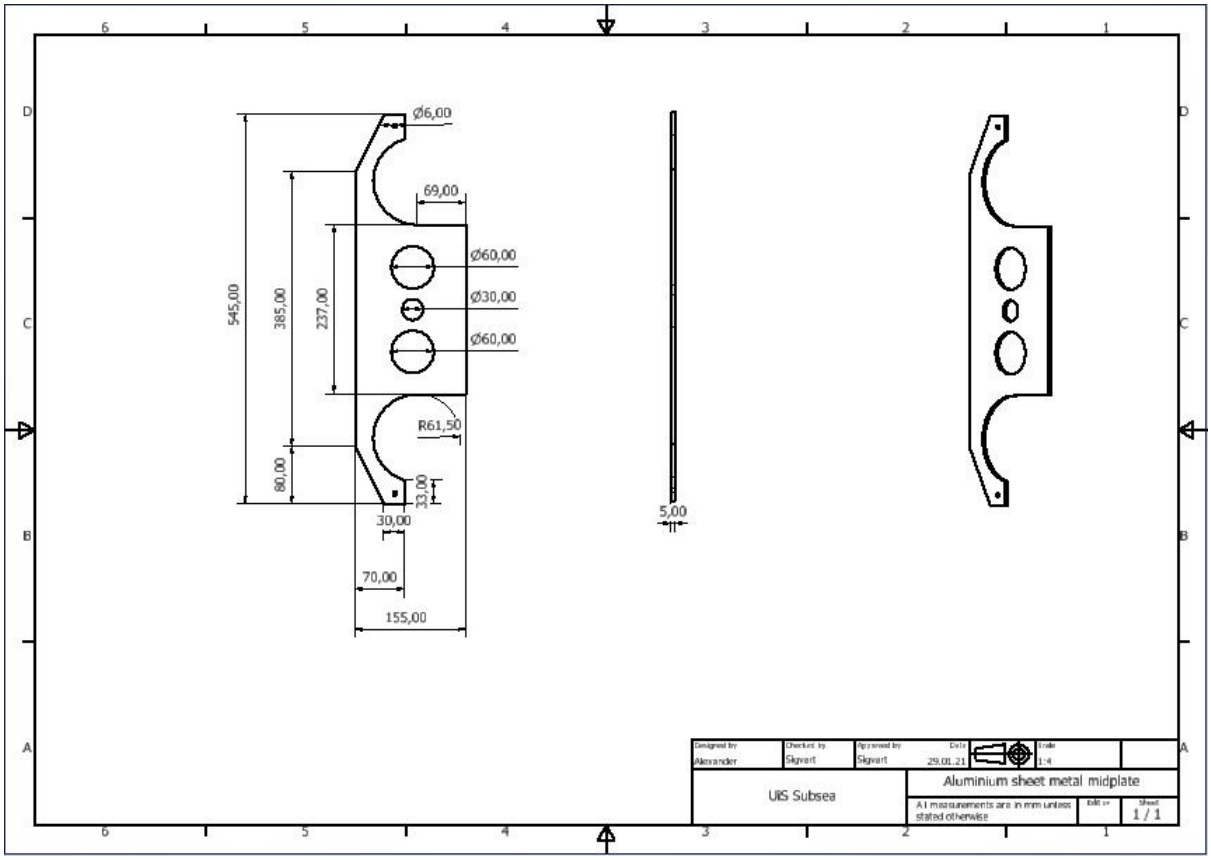


*Figure A.8 – Technical drawing of one mid-plate component*

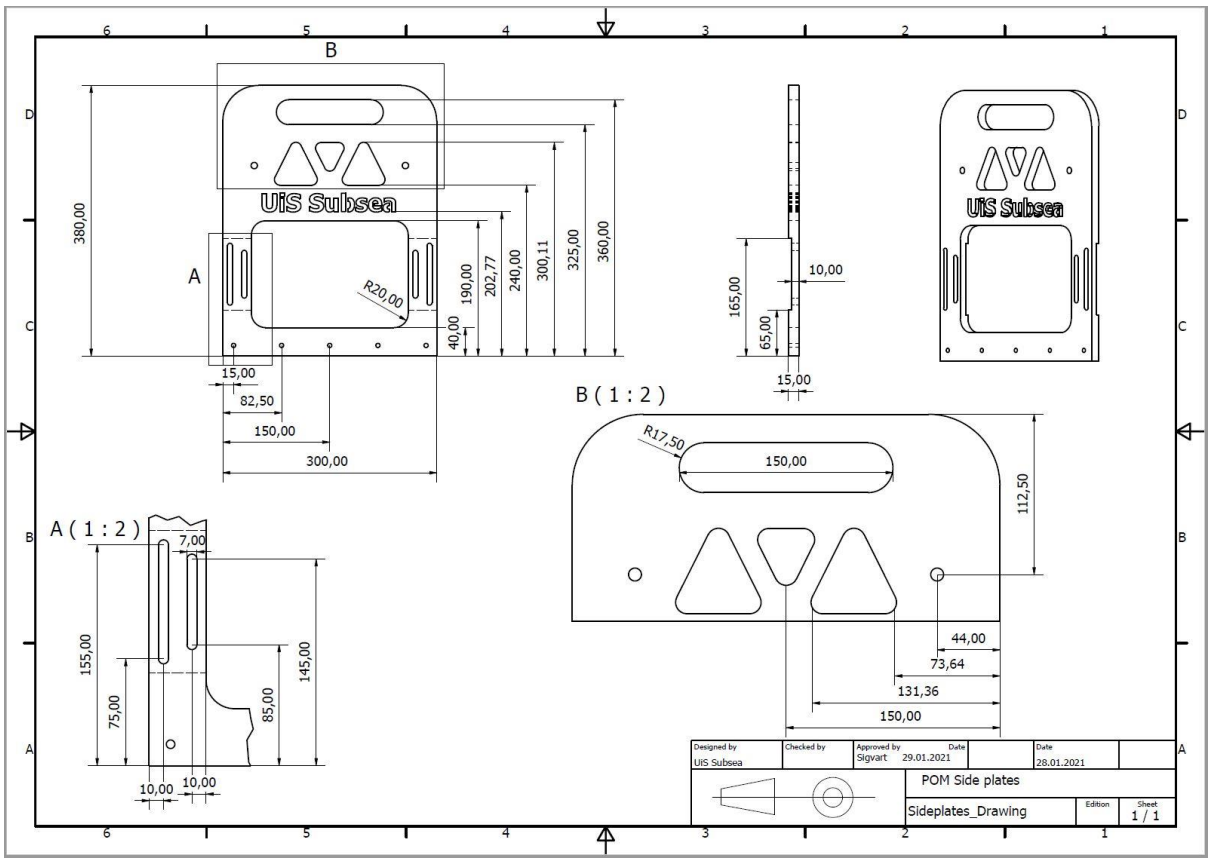


*Figure A.9 – Technical drawing of side plate*

# Bibliography


Barton, J. A., Love, D. M. & Taylor, G. D., 2001. *Design determines 70% of cost? A review of implications for design evaluation,* s.l.: Taylor & Francis.

Callister, Jr., W. D. & Rethwisch, D. G., 2014. *Materials Science and Engineering.* Ninth Edition ed. New York: Wiley.

Carlton, J., 2012. Propulsion systems. In: *Marine Propellers and Propulsion (Third Edition).* s.l.:s.n.

Chemistry LibreTexts, 2020. *Sacrificial Anode.* [Online]
Available at:
https://chem.libretexts.org/Bookshelves/Analytical_Chemistry/Supplemental_Modules_(Analytical_Chemistry)/Electrochemistry/Exemplars/Corrosion/Sacrificial_Anode
[Accessed 19 04 2021].

Ezpeleta, I., Justel, D., Bereau, U. & Zubelzu, J., 2019. *DFA-SPDP, a new DFA method to improve the assembly during all the product development phases,* Mondragon: Mondragon Unibertsitatea, Faculty of Engineering, Mechanical and Industrial Production.

Gokhare, V., Raut, D. D. N. & Shinde, D. D. K., 2017. *A Review paper on 3D-Printing Aspects and Various Processes Used in the 3D-Printing,* Mumbai: International Journal of Engineering Research & Technology (IJERT).

Gudmundsson, S., 2014. *General aviation aircraft design; Applied Methods and Procedures.* First edition ed. Oxford, UK: Butterworth-Heinemann.

Hambley, A. R., 2018. *Electrical Engineering Principles and Applications.* Seventh Edition ed. Harlow: Pearson Education Limited.

Härkegård, G., 2004. *Dimensjonering av maskindeler.* 1. ed. Trondheim: Fagbokforlaget.

Koh K. K., *. O. Y. A. E. N. K., 2015. The Study of Ducted Propeller in Propulsion Performance of a Malaysia Fishing Boat. *The Study of Ducted Propeller in Propulsion Performance of a Malaysia Fishing Boat*, 15 05, pp. 1-6.

Lemu, H. G., 2020. *Dimensjonering av maskinelementer.* Stavanger: UiS, Department of Structural Engineering and Materials Technology.

Lincoln Electric, 2021. *A Guide to Aluminium Welding.* [Online]
Available at: https://www.lincolnelectric.com/en-gb/support/welding-how-to/Pages/guide-aluminum-welding-detail.aspx
[Accessed 12 03 2021].

Marine, M., 2004. [Online]
Available at: argonaute.pagesperso-orange.fr/Helice.pdf
[Accessed 11 04 2021].

Marsh Fasteners, 2020. *Can Stainless Steel And Aluminum Be Used Together?.* [Online]
Available at: https://www.marshfasteners.com/can-stainless-steel-and-aluminum-be-used-together/
[Accessed 16 04 2021].

MATE Inspiration for Innovation, 2021. *MATE Regional ROV Competition Network.* [Online]
Available at: https://materovcompetition.org/regionals
[Accessed 15 01 2021].

MATE Inspiration for Innovation, 2021. *MATE ROV Competition.* [Online]
Available at: https://files.materovcompetition.org/2021/2021_EXPLORER_Manual_8Mar2021.pdf
[Accessed 15 01 2021].

MatWeb - Material Property Data, 2021. *MatWeb, Your Source for Materials Information.* [Online]
Available at: http://www.matweb.com/index.aspx
[Accessed 13 05 2021].

Oceaneering, 2021. *ROV Systems.* [Online]
Available at: https://www.oceaneering.com/rov-services/rov-systems/
[Accessed 16 01 2021].

Photocentric, 2021. *LC Magna.* [Online]
Available at: https://photocentricgroup.com/lcmagna/
[Accessed 03 04 2021].

Stienstra, D., n.d. *Gatech.edu.* [Online]
Available at:
https://www.google.com/url?sa=t&rct=j&q=&esrc=s&source=web&cd=&ved=2ahUKEwj6jZbD4LnwAhUsmIsKHXKkA2cQFjAAegQIAxAD&url=https%3A%2F%2Fme.gatech.edu%2Ffiles%2Fcapstone%2FL071ME4182DFA&usg=AOvVaw1wzH6kG_VqFojY4ELtIrrz
[Accessed 08 05 2021].

The Mariners' Museum and Park, 2021. *ROV.* [Online]
Available at: https://exploration.marinersmuseum.org/object/rov/
[Accessed 15 01 2021].

The Open University, 2018. *Gas shielded arc welding processes.* [Online]
Available at: https://www.open.edu/openlearn/science-maths-technology/engineering-technology/manupedia/gas-shielded-arc-welding-processes-tig/mig/mag
[Accessed 10 05 2021].

UiS Subsea, 2021. *Vehicles.* [Online]
Available at: https://sites.google.com/view/uissubsea/about-us/vehicles
[Accessed 15 01 2021].

Ulgen, M. N., 2013. *Google Patents.* Istanbul, Patent No. US 9,611,020 B2.

Ulrich, K. T. & Eppinger, S. D., 2016. *Product Design and Development.* Sixth Edition ed. New York: McGraw-Hill Education.

Yedamale, P., 2009. *Brushless DC (BLDC) Motor Fundamentals.* [Online]
Available at: https://www.eetimes.com/brushless-dc-bldc-motor-fundamentals/
[Accessed 18 04 2021].

Øydegard, P., 2014. *Design and dimensioning of the framework for an ROV,* Stavanger: University of Stavanger.